

**Synthesis of  $\text{Cu}_{0.5}\text{Mg}_{1.5}\text{Mn}_{0.5}\text{Al}_{0.5}\text{O}_x$  Mixed Oxide from Layered Double Hydroxide Precursor as Highly Efficient Catalyst for Low-temperature Selective Catalytic Reduction of  $\text{NO}_x$  with  $\text{NH}_3$**

Qinghua Yan<sup>1</sup>, Sining Chen<sup>1</sup>, Cheng Zhang<sup>1</sup>, Dermot O'Hare<sup>2</sup>, and Qiang Wang<sup>1,\*</sup>

<sup>1</sup>College of Environmental Science and Engineering, Beijing Forestry University, 35 Qinghua East Road, Haidian District, Beijing 100083, P. R. China

<sup>2</sup>Chemistry Research Laboratory, Department of Chemistry, University of Oxford, 12 Mansfield Road, Oxford, OX1 3TA, UK

\*Corresponding author:

College of Environmental Science and Engineering,

Beijing Forestry University,

Beijing 100083 (P. R. China)

Tel: +86 13699130626

E-mail: [qiang.wang.ox@gmail.com](mailto:qiang.wang.ox@gmail.com); [qiangwang@bjfu.edu.cn](mailto:qiangwang@bjfu.edu.cn)

## Abstract

We report a novel NH<sub>3</sub>-SCR catalyst Cu<sub>0.5</sub>Mg<sub>1.5</sub>Mn<sub>0.5</sub>Al<sub>0.5</sub>O<sub>x</sub> synthesized from layered double hydroxides with superior activity in a wide temperature range and improved SO<sub>2</sub> and H<sub>2</sub>O resistance comparing to conventional doped Mn/ $\gamma$ -Al<sub>2</sub>O<sub>3</sub>. This catalyst results in a high NO<sub>x</sub> removal efficiency of 87.0%–96.6% in the low temperature range of 100–250 °C, much better than Mn/ $\gamma$ -Al<sub>2</sub>O<sub>3</sub> (35.0%–67.2%). Besides, it exhibits significant resistance to SO<sub>2</sub> and H<sub>2</sub>O due to the existence of Cu and Mg. The promoting effects of Cu and Mg are thoroughly investigated using various physico-chemical techniques. The superior NH<sub>3</sub>-SCR activity of Cu<sub>0.5</sub>Mg<sub>1.5</sub>Mn<sub>0.5</sub>Al<sub>0.5</sub>O<sub>x</sub> catalyst can be associated with its high specific surface area, high reducibility of MnO<sub>2</sub> and CuO species, abundance of acid sites, and the well dispersion of MnO<sub>2</sub> and CuO species. The interactions between SO<sub>2</sub> and NH<sub>3</sub>, and the degradation mechanism caused by SO<sub>2</sub> were investigated using in-situ DRIFT analysis.

**Keywords:** NH<sub>3</sub>-SCR, Mn-based catalyst, layered double hydroxides, sulfur dioxide, regenerability

## 1. Introduction

The detrimental effects of nitrogen oxides ( $\text{NO}_x$ ) including the formations of photochemical smog, acid rain, ozone depletion and greenhouse as well as direct negative effects on the human respiratory system have been well recognized [1]. For  $\text{NO}_x$  emission control from stationary flue gases, selective catalytic reduction of  $\text{NO}_x$  by  $\text{NH}_3$  ( $\text{NH}_3$ -SCR) has been considered as one of the most effective and widely commercialized techniques [2]. During the past decade, Mn-based catalysts have attracted considerable attention due to their high  $\text{NO}_x$  conversion at low temperatures [3-10], however, they also possess some drawbacks, e.g. low activity at high-temperatures, susceptible to  $\text{SO}_2$  poisoning, and easy sintering, etc. [3, 11].

Layered double hydroxides (LDHs) are a new type of inorganic functional materials [12-15]. Recently, LDHs derived mixed oxides have been widely used in a variety of catalytic applications thanks for their large specific surface area (SSA), good thermal stability, and high metal dispersion [16, 17]. Using this approach, the dispersion of active metal species can be controlled at atomic level. Therefore, LDHs have been considered as good precursors for the preparation of Mn-based catalysts by calcination, which has the chance to solve the problems of sintering and dispersion of active components. In view of the good performance of Cu-based SCR catalysts at medium-high temperatures [18, 19], the introduction of Cu into Mn-based catalysts is considered to be able to broaden the reaction temperature window. Considering the fact that Mg has good trapping performance of acidic gases [13, 20], the introduction of Mg into Mn-based catalysts might be able to improve the sulfur resistance. In addition, to improve the stability of the LDHs material itself, certain amount of Al will be needed as well.

Based on the above concepts, and according to the existing problems of Mn-based SCR catalysts, we designed a novel catalyst  $\text{Cu}_w\text{Mg}_{2-w}\text{Mn}_y\text{Al}_{1-y}\text{O}_x$  from LDHs containing both Cu, Mg, Mn, and Al metals. We suspect that the resulting highly dispersed  $\text{MnO}_x$  and  $\text{CuO}_x$  species could provide good catalytic activity at low and medium-high temperatures, respectively. And the resulting highly dispersed MgO and  $\text{Al}_2\text{O}_3$  could provide good sulfur resistance and high thermal stability of catalyst,

respectively. This newly designed NH<sub>3</sub>-SCR catalyst is expected to have good De-NO<sub>x</sub> activity in a wider temperature window, higher sulfur resistance and stability than the conventional doped type Mn-based catalysts. Both the designing principal and the superior performance of the resulting multifunctional NH<sub>3</sub>-SCR catalysts are considered as important breakthroughs in this field.

## 2. Experimental

### 2.1. Preparation of catalysts

A standard co-precipitation method was used to synthesize Cu<sub>w</sub>Mg<sub>2-w</sub>Mn<sub>y</sub>Al<sub>1-y</sub>-CO<sub>3</sub> LDH precursors, and the M<sup>2+</sup>/M<sup>3+</sup> molar ratio is 2 (M<sup>2+</sup> represents divalent cations Cu<sup>2+</sup> and Mg<sup>2+</sup>; M<sup>3+</sup> represents trivalent cations Mn<sup>3+</sup> and Al<sup>3+</sup>). First, a metal aqueous solution containing the desired amounts of Mg(NO<sub>3</sub>)<sub>2</sub>·6H<sub>2</sub>O, Cu(NO<sub>3</sub>)<sub>2</sub>·6H<sub>2</sub>O, Al(NO<sub>3</sub>)<sub>3</sub>·9H<sub>2</sub>O, and 50% Mn(NO<sub>3</sub>)<sub>2</sub> was evenly added drop-wise to a Na<sub>2</sub>CO<sub>3</sub> solution (100 mL) under vigorously stirring at 60 °C. During the synthesis, the pH of the mixture solution was maintained constant at 10 by drop-wise addition of a solution of NaOH (4 M). In order to oxidize Mn<sup>2+</sup> to Mn<sup>3+</sup>, the solution was bubbled with air during the whole aging step. After that, the slurry was continuously stirred at 60 °C for another 12 h. After aging, the precipitate was filtered and washed for several times with deionized water until pH = 7. The LDH slurry was washed with acetone for 2 h and then dried at 60 °C in an oven for 24 h. The samples were denoted Cu<sub>w</sub>Mg<sub>2-w</sub>Mn<sub>y</sub>Al<sub>1-y</sub>-CO<sub>3</sub> LDH (0 < y < 1, 0 < w < 2). Finally, the Cu<sub>w</sub>Mg<sub>2-w</sub>Mn<sub>y</sub>Al<sub>1-y</sub>-CO<sub>3</sub> LDH solids were then calcined, the temperature is 400 °C for 5 h, obtaining the corresponding Cu<sub>w</sub>Mg<sub>2-w</sub>Mn<sub>y</sub>Al<sub>1-y</sub>O<sub>x</sub> catalysts. In addition, 2 wt% Mn/γ-Al<sub>2</sub>O<sub>3</sub> catalyst was prepared by a conventional incipient wetness impregnation method for comparison. 2.5 g γ-Al<sub>2</sub>O<sub>3</sub> solid was impregnated with 10 mL aqueous solution containing 0.2 mL 50% Mn(NO<sub>3</sub>)<sub>2</sub>.

### 2.2. Characterizations of catalysts

X-ray diffraction (XRD) analyses were conducted on a Shimadzu XRD-7000 instrument in reflection mode with Cu Kα radiation (λ = 1.542 Å). The accelerating voltage was set at 40 kV with 30 mA current. The diffraction patterns were recorded within the 2θ ranging from 5° to 70° with the setting

scan speed of 5°/min and a step size of 0.02°. The SSA of  $\text{Cu}_w\text{Mg}_{2-w}\text{Mn}_y\text{Al}_{1-y}\text{-CO}_3$  LDHs and  $\text{Cu}_w\text{Mg}_{2-w}\text{Mn}_y\text{Al}_{1-y}\text{O}_x$  was obtained through Brunauer–Emmett–Teller (BET) method, with a physisorption analyser (SSA–7000, Builder). The morphology of  $\text{Cu}_w\text{Mg}_{2-w}\text{Mn}_y\text{Al}_{1-y}\text{-CO}_3$  LDHs were characterized using field emission scanning electron microscope (FE-SEM, SU-8010, Hitachi). TEM analyses were performed on JEM-2100 microscope (JEOL, Japan), and the accelerating voltage is 200 kV. High resolution transmission electron microscopy (HR-TEM) analyses were performed on Tecnai G<sup>2</sup> F20 (FEI, USA), and the accelerating voltage is 200 kV.

Fourier transform infrared spectrometer (FT-IR) experiments were implemented on a FTS 3000 MX FT-IR (Bruker Vertex 70) spectrophotometer using diamond ATR technique. The in situ DRIFT characterization were also implemented on the FTS 3000 MX FTIR (Bruker Vertex 70) spectrophotometer with a reaction cell (ZnSe windows) and a diffuse reflectance attachment (HARRICK). The resolution is 4 cm<sup>-1</sup>, the number of scans is 32, and the spectrum is expressed as Kubelka–Munk function called the background spectrum of catalyst recorded in N<sub>2</sub>. For the NH<sub>3</sub> adsorption experiments, NH<sub>3</sub> was injected for 30 min at 150 °C and the corresponding spectra were recorded over time; for the interaction between SO<sub>2</sub> and NH<sub>3</sub> experiments, DRIFT spectra was collected while the sample was exposed to 1000 ppm NH<sub>3</sub>+500 ppm SO<sub>2</sub>, in the presence of 5% O<sub>2</sub>, at 150 °C for 30 min. The FTIR spectra of chemisorbed pyridine was collected for characterization of acidity using a Thermo Nicolet 380 spectrometer. 0.02 g of catalyst was pressed into disks and pretreated for 1 h at 400 °C under vacuum condition. When catalyst was saturated with pyridine vapor for 30 min at 40 °C, the pyridine desorption is executed at 150 °C, and the spectra were recorded simultaneously.

The NH<sub>3</sub>-TPD experiments were performed to measure the acidity of catalysts. The experiments were implemented on a multifunction chemisorption analyzer (PCA-1200, Builder) with thermal conductivity detector (TCD). For each measurement, 0.05 g catalyst was charged. Before each experiment, catalyst was pretreated at 200 °C in Ar (30 ml/min) for 30 min. The catalyst temperature was reduced to 100 °C, and then the catalyst was exposed to pure NH<sub>3</sub> (30 ml/min) for 1 h. In addition,

the physical adsorption of  $\text{NH}_3$  was removed by Ar purification for 1 h before  $\text{NH}_3$ -TPD experiments. The catalyst in Ar (30 ml/min) from 100 to 600 °C with a heating rate of 10 °C/min was recorded and finally maintained at 600 °C for 10 min.  $\text{H}_2$ -TPR analysis were performed on a multifunction chemisorption analyzer (PCA-1200, Builder). Prior to the experiments, approximately 0.05 g of samples were activated under Argon (30 ml/min) for 1 h at 200 °C and the catalyst temperature was reduced to 100 °C. As the reducing gas, 10 vol.%  $\text{H}_2$  in Ar (30 ml/min) was elected to reduce the catalyst from 100 to 600 °C, and the heating rate of is 10 °C/min.

XPS analysis were performed to determine the state of elements and atomic concentration on the surface of catalysts by a Thermo Scientific Escalab 250Xi instrument. The monochromatic Al  $K\alpha$  radiation (1486.6 eV) operate at a 15 kW accelerating power. Prior to each measurement, the catalyst was degassed at room temperature in the UHV chamber ( $<5 \times 10^{-7}$  Pa). The charge effect of catalysts was compensated, and all binding energies (BE) were calibrate with an adventitious C1s peak of 284.6 eV. This reference gave a BE value with an accuracy of  $\pm 0.1$  eV. The concentrations of Cu, Mn, and O on the sample surface were calculated from the integral of peak areas of the XPS data divided by each sensitivity factor of the elements. The total contents of Cu and Mn were detected using an inductively coupled plasma mass spectrometer (ICP-MS, Agilent 7900, USA). Electron spin resonance (ESR) spectra was recorded on a JES-FA200 spectrometer. The spectra was recorded at -170 °C temperature.

### **2.3. The catalytic activity tests**

$\text{NH}_3$ -SCR of  $\text{NO}_x$  was performed on a fixed-bed quartz reactor (i.d. 10 mm) including 0.15 g of catalyst. In each test, the composition of the reaction gas is 500 ppm  $\text{NO}_x$ , 500 ppm  $\text{NH}_3$ , 5%  $\text{O}_2$ , and balanced Ar. The total flow rate is 200 ml/min and GHSV=60,000  $\text{h}^{-1}$ . To study the effect of different GHSVs on the catalyst, the total flow rate is 350 ml/min and GHSV=105,000  $\text{h}^{-1}$ . Then the catalytic performance of samples were tested at different reaction temperatures and the feed gases were fed to the reactor. All the reaction gas flows were controlled independently by mass flow controllers (Brooks Instruments). The concentrations of NO and  $\text{NO}_2$  were continuously monitored by an on-line NO/ $\text{NO}_x$

analyzer (Thermo Scientific 42i-HL, USA). The N<sub>2</sub> selectivity was evaluated through a quadrupole mass spectrometer (QGA, Hidden, UK).

### 3. Results and discussion

#### 3.1. Characterization of Cu<sub>w</sub>Mg<sub>2-w</sub>Mn<sub>y</sub>Al<sub>1-y</sub>-CO<sub>3</sub> LDHs

The successful synthesis of Cu<sub>2-w</sub>Mg<sub>w</sub>Mn<sub>0.5</sub>Al<sub>0.5</sub>-CO<sub>3</sub> LDHs was verified by XRD analyses. Fig. 1(a) shows all Cu<sub>2-w</sub>Mg<sub>w</sub>Mn<sub>0.5</sub>Al<sub>0.5</sub>-CO<sub>3</sub> LDHs with different molar ratios of *w* ranging from 0 to 2 have a layered structure similar to Mg-Al-CO<sub>3</sub> LDHs [13]. Narrow and strong Bragg diffractions were observed, and the reflections at  $2\theta = 11.43^\circ$ ,  $23.10^\circ$ ,  $34.61^\circ$ ,  $39.15^\circ$ ,  $46.58^\circ$ ,  $60.21^\circ$ , and  $61.73^\circ$  may be indexed as the reflections of (003), (006), (012), (015), (018), (110), and (113) planes, respectively. The line widths indicated that these materials were of high crystalline. The FT-IR spectra of Cu<sub>2-w</sub>Mg<sub>w</sub>Mn<sub>0.5</sub>Al<sub>0.5</sub>-CO<sub>3</sub> LDHs is shown in Fig. 1(b). A broad absorption band centered at  $3451\text{ cm}^{-1}$  was attributed to the stretching vibrations of –OH groups in the brucite-like layers, the lattice water and the interlayer water molecules [21, 22]. The vibrations of angular deformation of H<sub>2</sub>O molecules were observed at  $1488$  and  $1556\text{ cm}^{-1}$  [22]. The absorption at  $1363\text{ cm}^{-1}$  was attributed to the vibrations of carbonate ions in the spectrum. Finally, the absorption bands around  $850$ ,  $728$ , and  $624\text{ cm}^{-1}$  were assigned to the vibrations of M–O (O–M–O, M–O–M or M–OH) [13]. Both XRD and FTIR data confirmed the successful synthesis of Cu<sub>2-w</sub>Mg<sub>w</sub>Mn<sub>0.5</sub>Al<sub>0.5</sub>-CO<sub>3</sub> LDHs. The morphology of LDHs was revealed by SEM and TEM analyses. Fig. 1(c, d) show that Cu<sub>0.5</sub>Mg<sub>1.5</sub>Mn<sub>0.5</sub>Al<sub>0.5</sub>-CO<sub>3</sub> LDH possesses typical “flower-like” morphology, with nanoplatelets assembled together. This similar morphology of Mg-Al LDHs had also been observed by Gennequin et al. [16].

#### 3.2. SCR activity of Cu<sub>w</sub>Mg<sub>2-w</sub>Mn<sub>0.5</sub>Al<sub>0.5</sub>O<sub>x</sub> and 2 wt% Mn/γ-Al<sub>2</sub>O<sub>3</sub> catalysts

To find out the optimal ratio of Cu<sup>2+</sup>/Mg<sup>2+</sup>, the NO<sub>x</sub> conversions as a function of reaction temperature over Cu<sub>2-w</sub>Mg<sub>w</sub>Mn<sub>0.5</sub>Al<sub>0.5</sub>O<sub>x</sub> catalysts are shown in Fig. 2(a). The NO<sub>x</sub> conversions of all samples first increased with the increase of temperature from 100 to 150 °C and then started to decrease with a further increase of temperature to 300 °C. Particularly the Cu<sub>0.5</sub>Mg<sub>1.5</sub>Mn<sub>0.5</sub>Al<sub>0.5</sub>O<sub>x</sub> catalyst exhibited

outstanding NH<sub>3</sub>-SCR activity in a wide range of 100–250 °C. The maximum NO<sub>x</sub> conversion of catalysts followed the order of Cu<sub>0.5</sub>Mg<sub>1.5</sub>Mn<sub>0.5</sub>Al<sub>0.5</sub>O<sub>x</sub> (96.7%) > Mg<sub>2</sub>Mn<sub>0.5</sub>Al<sub>0.5</sub>O<sub>x</sub> (93.3%) > Cu<sub>1</sub>Mg<sub>1</sub>Mn<sub>0.5</sub>Al<sub>0.5</sub>O<sub>x</sub> (92.2%) > Cu<sub>1.5</sub>Mg<sub>0.5</sub>Mn<sub>0.5</sub>Al<sub>0.5</sub>O<sub>x</sub> (91.3%) > Cu<sub>2</sub>Mn<sub>0.5</sub>Al<sub>0.5</sub>O<sub>x</sub> (91.2%) > Mn/γ-Al<sub>2</sub>O<sub>3</sub> (67.2%). With the increase of *w* value from 0 to 0.5, the NO<sub>x</sub> conversion increased and the effective temperature range was expanded. However, further increasing the *w* value from 0.5 to 2 resulted in a decrease in NO<sub>x</sub> conversion in both low and high reaction temperature ranges. Previous studies have proven that there is always a maximum loading of active component for conventional doped catalysts [23, 24]. When the active component loading exceeds its maximum value, sintering and crystallization of active components will occur, consequently reducing the activity of catalyst [23]. Thus, Cu<sub>0.5</sub>Mg<sub>1.5</sub>Mn<sub>0.5</sub>Al<sub>0.5</sub>O<sub>x</sub> catalyst showed the best SCR catalytic activity, with the NO<sub>x</sub> conversion being maintained above 87.2% over the entire temperature range of 100–250 °C, and the highest NO<sub>x</sub> conversion of 96.7% at 150 °C. However, the highest NO<sub>x</sub> removal efficiency of the traditional Mn-based catalyst (Mn/γ-Al<sub>2</sub>O<sub>3</sub>) is only 67.2% at 200 °C. As NH<sub>3</sub> might be oxidized during the SCR reaction, the N<sub>2</sub> selectivity was also considered (Fig. 2(b)). Mn/γ-Al<sub>2</sub>O<sub>3</sub> catalyst showed the lowest N<sub>2</sub> selectivity, and Cu<sub>0.5</sub>Mg<sub>1.5</sub>Mn<sub>0.5</sub>Al<sub>0.5</sub>O<sub>x</sub> showed an excellent N<sub>2</sub> selectivity and activity in the whole testing temperature range of 100–300 °C. Thus, it can be concluded that both the catalytic activity and N<sub>2</sub> selectivity were improved at 100–300 °C by the introduction Cu and Mg. Fig. 2(c) indicates the Cu<sub>0.5</sub>Mg<sub>1.5</sub>Mn<sub>0.5</sub>Al<sub>0.5</sub>O<sub>x</sub> catalyst has a better tolerance to the effect of different GHSVs than Mn/γ-Al<sub>2</sub>O<sub>3</sub> catalyst. The NO<sub>x</sub> conversion of Cu<sub>0.5</sub>Mg<sub>1.5</sub>Mn<sub>0.5</sub>Al<sub>0.5</sub>O<sub>x</sub> only slightly decreased with increasing the GHSV from 60,000 to 105,000 h<sup>-1</sup>, and still maintained high NO<sub>x</sub> conversions in the low temperature range of 100–200 °C. These results indicated that the addition of Cu can not only improve the activity, but also widen the active reaction temperature range of the Mn-based NH<sub>3</sub>-SCR catalysts.

In order to understand why Cu<sub>0.5</sub>Mg<sub>1.5</sub>Mn<sub>0.5</sub>Al<sub>0.5</sub>O<sub>x</sub> catalyst has better activity than other catalysts, the XRD patterns of these catalysts were recorded (Fig. 2(d)). After 400 °C calcination, both Mn/γ-Al<sub>2</sub>O<sub>3</sub> and Cu<sub>w</sub>Mg<sub>2-w</sub>Mn<sub>0.5</sub>Al<sub>0.5</sub>O<sub>x</sub> were converted to a mixture of oxides and spinels. For



Mn/ $\gamma$ -Al<sub>2</sub>O<sub>3</sub>, the diffraction peaks can be attributed to crystallized MnO<sub>2</sub> (JCPDS No. 24-0735). For Cu<sub>2</sub>Mn<sub>0.5</sub>Al<sub>0.5</sub>O<sub>x</sub>, the peaks at 35.5° and 38.7° can be assigned to CuO phase (JCPDS No. 48-1548), the peaks at 28.7°, 42.7°, and 56.7° can be assigned to MnO<sub>2</sub>, and a small amount of CuMn<sub>2</sub>O<sub>4</sub>-like spinel (JCPDS No. 34-1400) was also detected. For Cu<sub>0.5</sub>Mg<sub>1.5</sub>Mn<sub>0.5</sub>Al<sub>0.5</sub>O<sub>x</sub>, both CuO and MnO<sub>2</sub> phases were detected, together with a small amount of MgO (JCPDS No. 30-0794). For Mg<sub>2</sub>Mn<sub>0.5</sub>Al<sub>0.5</sub>O<sub>x</sub>, periclase type MgO and MnO<sub>2</sub> were observed. Besides, MgMn<sub>2</sub>O<sub>4</sub>-like spinel (JCPDS No. 23-0392) was formed with the peaks appearing at 30.8°, 36.3°, 58.4°, and 64.2°. However, aluminum oxide was not detected, indicating an amorphous state.

The physical properties of the LDHs derived Cu<sub>w</sub>Mg<sub>2-w</sub>Mn<sub>0.5</sub>Al<sub>0.5</sub>O<sub>x</sub> and Mn/ $\gamma$ -Al<sub>2</sub>O<sub>3</sub> were evaluated by BET measurements (Table 1). Obviously, Cu<sub>w</sub>Mg<sub>2-w</sub>Mn<sub>0.5</sub>Al<sub>0.5</sub>O<sub>x</sub> possesses larger SSA than Mn/ $\gamma$ -Al<sub>2</sub>O<sub>3</sub>, which is favorable for improving SCR activity by providing more available active binding/sorption sites for reactants [25-27]. Cu<sub>0.5</sub>Mg<sub>1.5</sub>Mn<sub>0.5</sub>Al<sub>0.5</sub>O<sub>x</sub> catalyst exhibited the largest SSA (228.7 m<sup>2</sup>/g) [28]. Thus, it might be one of the reasons that Cu<sub>0.5</sub>Mg<sub>1.5</sub>Mn<sub>0.5</sub>Al<sub>0.5</sub>O<sub>x</sub> catalyst exhibits the best activity. The microstructures of Mn/ $\gamma$ -Al<sub>2</sub>O<sub>3</sub> and Cu<sub>0.5</sub>Mg<sub>1.5</sub>Mn<sub>0.5</sub>Al<sub>0.5</sub>O<sub>x</sub> were further studied by HR-TEM analysis. For Mn/ $\gamma$ -Al<sub>2</sub>O<sub>3</sub>, MnO<sub>2</sub> nanoparticles with fringe spacing of 0.311 nm, referring to its (110) crystal plane were observed (Fig. 3(a)). For Cu<sub>0.5</sub>Mg<sub>1.5</sub>Mn<sub>0.5</sub>Al<sub>0.5</sub>O<sub>x</sub>, “flower-like” hierarchical morphology was observed in Fig. 3(b–d). Fringe spacings of 0.23, 0.21, 0.29, and 0.31 nm which correspond to the (111) crystal plane of CuO, (200) plane of MgO, (220) plane of CuMn<sub>2</sub>O<sub>4</sub>, and (112) plane of MgMn<sub>2</sub>O<sub>4</sub> were observed, respectively. These results are consistent with XRD patterns in Fig. 2(d), in which the characteristic diffraction patterns for CuO, MgO, CuMn<sub>2</sub>O<sub>4</sub>, and MgMn<sub>2</sub>O<sub>4</sub> were clearly identified.

The chemical composition and oxidation state of manganese and copper in different catalysts were examined using XPS analyses. Fig. 4 shows the XPS spectra of O 1s, Cu 2p, and Mn 2p of Mn/ $\gamma$ -Al<sub>2</sub>O<sub>3</sub>, Cu<sub>2</sub>Mn<sub>0.5</sub>Al<sub>0.5</sub>O<sub>x</sub>, Cu<sub>0.5</sub>Mg<sub>1.5</sub>Mn<sub>0.5</sub>Al<sub>0.5</sub>O<sub>x</sub>, and Mg<sub>2</sub>Mn<sub>0.5</sub>Al<sub>0.5</sub>O<sub>x</sub>. The surface chemical compositions of these samples are summarized in Table 2. By performing peak-fitting deconvolutions, the Mn 2p<sub>3/2</sub> can be divided into two characteristic peaks, which can be attributed to Mn<sup>4+</sup> (643.2 ±

0.2 eV) and  $\text{Mn}^{3+}$  ( $642.0 \pm 0.2$  eV), respectively [29]. The  $\text{NH}_3$ -SCR of  $\text{NO}_x$  over pure manganese oxides at low temperature was also studied by Kapteijn et al [30]. They found that the denitrification efficiency reduced in the order of  $\text{MnO}_2 > \text{Mn}_5\text{O}_8 > \text{Mn}_2\text{O}_3 > \text{Mn}_3\text{O}_4$ . The relative concentrations of  $\text{Mn}^{4+}$  in this research follows the order of  $\text{Cu}_{0.5}\text{Mg}_{1.5}\text{Mn}_{0.5}\text{Al}_{0.5}\text{O}_x > \text{Cu}_2\text{Mn}_{0.5}\text{Al}_{0.5}\text{O}_x > \text{Mg}_2\text{Mn}_{0.5}\text{Al}_{0.5}\text{O}_x > \text{Mn}/\gamma\text{-Al}_2\text{O}_3$ . Previous studies have demonstrated that  $\text{Mn}^{4+}$  possesses better redox properties of manganese-based catalysts [31, 32]. Thus, the high concentration of  $\text{Mn}^{4+}$  in  $\text{Cu}_{0.5}\text{Mg}_{1.5}\text{Mn}_{0.5}\text{Al}_{0.5}\text{O}_x$  catalyst is favorable for its excellent low-temperature SCR activity.

Fig. 4(b) shows the Cu 2p XPS spectra of  $\text{Cu}_2\text{Mn}_{0.5}\text{Al}_{0.5}\text{O}_x$  and  $\text{Cu}_{0.5}\text{Mg}_{1.5}\text{Mn}_{0.5}\text{Al}_{0.5}\text{O}_x$  samples. The satellite peaks at 938.0–945.0 eV and 960.0–965.0 eV, and the intense and broad photoelectron peaks at 934 eV (Cu 2p<sub>3/2</sub>) and 955.0 eV (Cu 2p<sub>1/2</sub>) were detected for all samples. In addition, the relative intensity of  $\text{Cu}^{2+}$  of  $\text{Cu}_{0.5}\text{Mg}_{1.5}\text{Mn}_{0.5}\text{Al}_{0.5}\text{O}_x$  (93%) is higher than that of  $\text{Cu}_2\text{Mn}_{0.5}\text{Al}_{0.5}\text{O}_x$  (91%), which is favorable for the high  $\text{NO}_x$  conversion activity.

Fig. 4(c) shows the O 1s XPS spectra of all catalysts. The lower binding energy peak at 528.7–530.9 eV corresponds to lattice oxygen ( $\text{O}_\alpha$ ), and the higher binding energy peak (531.4–532.5 eV) is related to the surface adsorbed oxygen ( $\text{O}_\beta$ ) [33]. It is worth to notice that the relative concentration ratio of  $\text{O}_\beta$  increased and reached the maximum value with  $\text{Cu}_{0.5}\text{Mg}_{1.5}\text{Mn}_{0.5}\text{Al}_{0.5}\text{O}_x$  catalyst (Table 2). This implies that the synthesis of  $\text{Cu}_{0.5}\text{Mg}_{1.5}\text{Mn}_{0.5}\text{Al}_{0.5}\text{O}_x$  mixed oxide from LDH can result in more surface oxygen vacancies. It has been reported that due to its higher mobility, the surface adsorbed oxygen ( $\text{O}_\beta$ ) plays a key role in the  $\text{NH}_3$ -SCR reaction [34, 35]. XPS analyses indicated that the high concentrations of  $\text{Mn}^{4+}$ ,  $\text{Cu}^{2+}$  and  $\text{O}_\beta$  should also be responsible for the good performance of  $\text{Cu}_{0.5}\text{Mg}_{1.5}\text{Mn}_{0.5}\text{Al}_{0.5}\text{O}_x$  catalyst. In our work, the existence of both  $\text{MnO}_2$  and  $\text{CuO}$  were clearly seen in the XRD analyses. The  $\text{MnO}_2$  and  $\text{CuO}$  nanoparticles were also observed in the HR-TEM. XPS analyses show that the relative concentration of  $\text{MnO}_2$  and  $\text{CuO}$  agreed well with their SCR activities. We confirmed that the presence of  $\text{MnO}_2$  and  $\text{CuO}$  are the main reason for its high activity through XRD, XPS and HR-TEM analyses, which was consistent with most previous studies. The Mn-based catalysts mainly containing  $\text{MnO}_2$  was preferred for good SCR performance. In addition, it was also

well believed that the high dispersed CuO species was advantageous to the catalytic reaction in Cu-based catalyst, particularly at low temperatures. In all, we are very confident to conclude that the highly dispersed MnO<sub>2</sub> and CuO are the active species for the good SCR performance of Cu<sub>0.5</sub>Mg<sub>1.5</sub>Mn<sub>0.5</sub>Al<sub>0.5</sub>O<sub>x</sub> catalyst.

Fig. 4(d) shows the ESR spectra of Cu<sub>0.5</sub>Mg<sub>1.5</sub>Mn<sub>0.5</sub>Al<sub>0.5</sub>O<sub>x</sub> and Mn/ $\gamma$ -Al<sub>2</sub>O<sub>3</sub> measured at -170 °C. The ESR spectra of Cu<sub>0.5</sub>Mg<sub>1.5</sub>Mn<sub>0.5</sub>Al<sub>0.5</sub>O<sub>x</sub> revealed the signal with *g* value of 2.004, which could be assigned to oxygen vacancy. However, no signal about oxygen vacancy was detected for Mn/ $\gamma$ -Al<sub>2</sub>O<sub>3</sub>. Oxygen vacancy could adsorb oxygen to produce reactive oxygen species and oxidized NO to produce nitro species, thereby facilitating the oxidation process in the SCR reaction. It was suggested that the presence of oxygen vacancy after Cu and Mg doping in Cu<sub>0.5</sub>Mg<sub>1.5</sub>Mn<sub>0.5</sub>Al<sub>0.5</sub>O<sub>x</sub> may be one of the reasons for its higher activity.

To elucidate the influence of various coordination structures on the adsorption property, turnover frequency (TOF) calculation can be helpful. To further verify the surface Cu<sup>2+</sup> and/or Mn<sup>4+</sup> species are the active sites for Cu<sub>2</sub>Mn<sub>0.5</sub>Al<sub>0.5</sub>O<sub>x</sub>, Cu<sub>0.5</sub>Mg<sub>1.5</sub>Mn<sub>0.5</sub>Al<sub>0.5</sub>O<sub>x</sub>, Mg<sub>2</sub>Mn<sub>0.5</sub>Al<sub>0.5</sub>O<sub>x</sub>, and Mn/ $\gamma$ -Al<sub>2</sub>O<sub>3</sub> catalysts, the TOF for NO<sub>x</sub> reaction based on Cu<sup>2+</sup> and/or Mn<sup>4+</sup> species was calculated and presented in Table 3. TOF is defined as the number of NO<sub>x</sub> molecules converted per Cu<sup>2+</sup>/Mn<sup>4+</sup> per second, as illustrated in equation (1), where X<sub>NO<sub>x</sub></sub> is NO<sub>x</sub> conversion (%) and F<sub>NO<sub>x</sub></sub> is the flow rate of NO<sub>x</sub> (L/min) [36]. The flow rate of NO<sub>x</sub> is corrected using the ideal gas law with the change in reaction temperature. The TOF based on surface Cu<sup>2+</sup>/Mn<sup>4+</sup> species displayed changes with the reaction temperature and NO<sub>x</sub> conversion. It can be seen that Cu<sub>0.5</sub>Mg<sub>1.5</sub>Mn<sub>0.5</sub>Al<sub>0.5</sub>O<sub>x</sub> catalyst exhibited a high TOF value in the range of 100–200 °C, which may explain its wide reaction temperature window. For Cu<sub>2</sub>Mn<sub>0.5</sub>Al<sub>0.5</sub>O<sub>x</sub>, Cu<sub>0.5</sub>Mg<sub>1.5</sub>Mn<sub>0.5</sub>Al<sub>0.5</sub>O<sub>x</sub>, and Mg<sub>2</sub>Mn<sub>0.5</sub>Al<sub>0.5</sub>O<sub>x</sub> catalysts, the maximum TOF values appeared at 150 °C. While for Mn/ $\gamma$ -Al<sub>2</sub>O<sub>3</sub>, its maximum TOF value appeared at 200 °C, which is consistent with the results of NO<sub>x</sub> conversion [36, 37]. However, for conventional supported catalysts, the loading is limited and excessive loading may lead to catalyst agglomeration, which affects its activity [23, 24]. Therefore, although Cu<sub>0.5</sub>Mg<sub>1.5</sub>Mn<sub>0.5</sub>Al<sub>0.5</sub>O<sub>x</sub> catalyst does not possess the highest

TOF value, it performs well in a wider reaction window.

$$\text{TOF} = X_{\text{NOx}} \times F_{\text{NOx}} / 60 \times 22.4 \times \text{amount of Cu}^{2+} (\text{Mn}^{4+}) \quad (1)$$

The chemical adsorption of pyridine coupled with FTIR spectroscopy is most widely used to probe the nature of the acid sites on catalyst surface. Fig. 5(a) shows the FTIR spectra of pyridine adsorbed on  $\text{Mg}_2\text{Mn}_{0.5}\text{Al}_{0.5}\text{O}_x$ ,  $\text{Cu}_{0.5}\text{Mg}_{1.5}\text{Mn}_{0.5}\text{Al}_{0.5}\text{O}_x$ ,  $\text{Cu}_2\text{Mn}_{0.5}\text{Al}_{0.5}\text{O}_x$ , and  $\text{Mn}/\gamma\text{-Al}_2\text{O}_3$ . The absorption peaks at 1450, 1490, 1573, and 1610  $\text{cm}^{-1}$  can be attributed to the pyridine coordinated on L acids, while the characteristic band at 1523  $\text{cm}^{-1}$  corresponds to B acid sites [38]. Peña et al.[39] reported that L acids are active but B acids may not contribute to the catalytic activity of SCR reaction. Yuan et al.[40] previously demonstrated that L acids are the adsorption sites for nitrate, which is the key intermediate for SCR. The concentration of L acids is proportional to the strength of the bands at 1444 and 1450  $\text{cm}^{-1}$  with a decreasing order of  $\text{Cu}_{0.5}\text{Mg}_{1.5}\text{Mn}_{0.5}\text{Al}_{0.5}\text{O}_x > \text{Mg}_2\text{Mn}_{0.5}\text{Al}_{0.5}\text{O}_x > \text{Cu}_2\text{Mn}_{0.5}\text{Al}_{0.5}\text{O}_x > \text{Mn}/\gamma\text{-Al}_2\text{O}_3$  [41, 42]. In order to quantitatively analyze the concentration of acid sites, the strength of the peaks at 1450 and 1444  $\text{cm}^{-1}$  was quantified for L acids. The relationship between the catalytic performance and the quantity of L acids is shown in Fig. 5(b). Apparently, the  $\text{Cu}_{0.5}\text{Mg}_{1.5}\text{Mn}_{0.5}\text{Al}_{0.5}\text{O}_x$  catalyst with the highest quantity of L acids resulted in best catalytic performance.

$\text{NH}_3$ -TPD analysis was then used to evaluate the surface acidity of catalysts. As shown in Fig. 5(c),  $\text{NH}_3$  desorption peak was detected over a wide temperature range, due to the variability of adsorbed  $\text{NH}_3$  species with different thermal stabilities. Two desorption peaks for  $\text{Cu}_{0.5}\text{Mg}_{1.5}\text{Mn}_{0.5}\text{Al}_{0.5}\text{O}_x$  and  $\text{Mg}_2\text{Mn}_{0.5}\text{Al}_{0.5}\text{O}_x$  were observed, which can be ascribed as the  $\text{NH}_3$  desorbed by acid sites. The desorption peak at high temperature (about 490  $^\circ\text{C}$ ) could be attributed to the  $\text{NH}_3$  desorbed by strong acid sites, which may be due to the introduction of Cu and Mg resulted in a change in the nature of the acid sites [37, 40]. The desorption peak at low temperature of all samples located at about 140  $^\circ\text{C}$  could be attributed to the  $\text{NH}_3$  desorbed by weak acid sites. The amounts of desorbed  $\text{NH}_3$  (surface acidity) over  $\text{Cu}_2\text{Mn}_{0.5}\text{Al}_{0.5}\text{O}_x$ ,  $\text{Cu}_{0.5}\text{Mg}_{1.5}\text{Mn}_{0.5}\text{Al}_{0.5}\text{O}_x$ ,  $\text{Mg}_2\text{Mn}_{0.5}\text{Al}_{0.5}\text{O}_x$ , and  $\text{Mn}/\gamma\text{-Al}_2\text{O}_3$  were compared by integrating the  $\text{NH}_3$ -TPD curves, and

$\text{Cu}_{0.5}\text{Mg}_{1.5}\text{Mn}_{0.5}\text{Al}_{0.5}\text{O}_x$  possessed much higher surface acidity than all other samples. The surface acidity of catalyst is considered to be closely relevant to the SCR catalytic activity [43, 44].

The redox property of catalysts is a key factor in determining the activity of  $\text{NH}_3$ -SCR. To figure out the effect of Cu and/or Mg on the redox ability of  $\text{Cu}_{0.5}\text{Mg}_{1.5}\text{Mn}_{0.5}\text{Al}_{0.5}\text{O}_x$ ,  $\text{H}_2$ -TPR analyses were performed. In Fig. 5(d), two reduction peaks were observed for  $\text{Mn}/\gamma\text{-Al}_2\text{O}_3$  and  $\text{Mg}_2\text{Mn}_{0.5}\text{Al}_{0.5}\text{O}_x$ , which can be attributed to the reduction of  $\text{MnO}_x$ . After the addition of Cu and/or Mg, the reduction peaks were lowered to 180 °C for  $\text{Cu}_{0.5}\text{Mg}_{1.5}\text{Mn}_{0.5}\text{Al}_{0.5}\text{O}_x$  and  $\text{Cu}_{0.5}\text{Mg}_{1.5}\text{Mn}_{0.5}\text{Al}_{0.5}\text{O}_x$  catalysts, which may be attributed to the good dispersion of  $\text{MnO}_x$  and the interaction with Cu. The broad reduction peaks (100–250 °C) of  $\text{Cu}_{0.5}\text{Mg}_{1.5}\text{Mn}_{0.5}\text{Al}_{0.5}\text{O}_x$  and  $\text{Cu}_{0.5}\text{Mg}_{1.5}\text{Mn}_{0.5}\text{Al}_{0.5}\text{O}_x$  catalysts could be assigned to the reduction of  $\text{MnO}_x$ , overlapped with the reduction of surface  $\text{Cu}^{2+}$  [45]. The  $\text{H}_2$  consumption peak of  $\text{Cu}_{0.5}\text{Mg}_{1.5}\text{Mn}_{0.5}\text{Al}_{0.5}\text{O}_x$  is obviously larger than that of  $\text{Cu}_2\text{Mn}_{0.5}\text{Al}_{0.5}\text{O}_x$ ,  $\text{Mg}_2\text{Mn}_{0.5}\text{Al}_{0.5}\text{O}_x$ , and  $\text{Mn}/\gamma\text{-Al}_2\text{O}_3$ , implying the introduction of Cu and Mg can increase the reducibility and catalytic activity of  $\text{Cu}_{0.5}\text{Mg}_{1.5}\text{Mn}_{0.5}\text{Al}_{0.5}\text{O}_x$  [46, 47].

### 3.3. Effect of $\text{H}_2\text{O}$ and $\text{SO}_2$

It is well accepted that SCR catalysts are normally poisoned by  $\text{H}_2\text{O}$  and  $\text{SO}_2$ . Thus, the effects of  $\text{H}_2\text{O}$  (5%) and  $\text{SO}_2$  (100 ppm) on the performance of our newly developed catalysts were also investigated. Fig. 6(a) shows the effect of individual  $\text{H}_2\text{O}$  on the performance of  $\text{Cu}_2\text{Mn}_{0.5}\text{Al}_{0.5}\text{O}_x$ ,  $\text{Cu}_{0.5}\text{Mg}_{1.5}\text{Mn}_{0.5}\text{Al}_{0.5}\text{O}_x$ ,  $\text{Mg}_2\text{Mn}_{0.5}\text{Al}_{0.5}\text{O}_x$ , and  $\text{Mn}/\gamma\text{-Al}_2\text{O}_3$  at 150 °C. In general, a visible decrease in  $\text{NO}_x$  removal efficiency was observed for all catalysts in the presence of 5% water vapor. Comparing to other catalysts,  $\text{Cu}_{0.5}\text{Mg}_{1.5}\text{Mn}_{0.5}\text{Al}_{0.5}\text{O}_x$  was less influenced, with the  $\text{NO}_x$  conversion remained as high as 78.2%, higher than that of  $\text{Cu}_2\text{Mn}_{0.5}\text{Al}_{0.5}\text{O}_x$  (66.3%),  $\text{Mg}_2\text{Mn}_{0.5}\text{Al}_{0.5}\text{O}_x$  (73.6%), and  $\text{Mn}/\gamma\text{-Al}_2\text{O}_3$  (37.2%). After stopping  $\text{H}_2\text{O}$  from the feed gases, the  $\text{NO}_x$  conversions can be restored to some extent, but still below the initial values, indicating that parts of the deactivation caused by  $\text{H}_2\text{O}$  is irreversible. The inhibiting effect of  $\text{H}_2\text{O}$  at low temperatures was mainly due to the competitive adsorption of  $\text{H}_2\text{O}$  at the same active sites [48, 49].

The individual effect of  $\text{SO}_2$  was also evaluated (Fig. 6(b)). At 150 °C, the  $\text{NO}_x$  removal

efficiency of  $\text{Mg}_2\text{Mn}_{0.5}\text{Al}_{0.5}\text{O}_x$ ,  $\text{Cu}_{0.5}\text{Mg}_{1.5}\text{Mn}_{0.5}\text{Al}_{0.5}\text{O}_x$ ,  $\text{Mg}_2\text{Mn}_{0.5}\text{Al}_{0.5}\text{O}_x$ ,  $\text{Cu}_2\text{Mn}_{0.5}\text{Al}_{0.5}\text{O}_x$ , and  $\text{Mn}/\gamma\text{-Al}_2\text{O}_3$  was decreased to 63.7%, 72.2%, 51.5%, and 41.5% after 1 h, and 47.4%, 69.2%, 35.6%, and 25.6% after 4 h, respectively. It can be concluded  $\text{Cu}_{0.5}\text{Mg}_{1.5}\text{Mn}_{0.5}\text{Al}_{0.5}\text{O}_x$  and  $\text{Mg}_2\text{Mn}_{0.5}\text{Al}_{0.5}\text{O}_x$  were much less effected by  $\text{SO}_2$  than  $\text{Cu}_2\text{Mn}_{0.5}\text{Al}_{0.5}\text{O}_x$  and  $\text{Mn}/\gamma\text{-Al}_2\text{O}_3$  catalysts, suggesting the  $\text{SO}_2$  resistance can be greatly improved by the introduction of Mg.

The inhibition effect by the co-existence of  $\text{SO}_2$  and  $\text{H}_2\text{O}$  was also studied at 150 °C (Fig. 6(c)). Once  $\text{SO}_2$  and  $\text{H}_2\text{O}$  were injected simultaneously, the  $\text{NO}_x$  conversion had a significant drop for all catalysts, indicating  $\text{SO}_2$  and  $\text{H}_2\text{O}$  had a great influence on  $\text{NO}_x$  conversion. After 2 h, the  $\text{NO}_x$  conversion of  $\text{Cu}_{0.5}\text{Mg}_{1.5}\text{Mn}_{0.5}\text{Al}_{0.5}\text{O}_x$ ,  $\text{Cu}_2\text{Mn}_{0.5}\text{Al}_{0.5}\text{O}_x$ ,  $\text{Mg}_2\text{Mn}_{0.5}\text{Al}_{0.5}\text{O}_x$ , and  $\text{Mn}/\gamma\text{-Al}_2\text{O}_3$  catalysts became 68.2%, 63.6%, 56%, and 33.3%, respectively. Upon removing  $\text{SO}_2$  and  $\text{H}_2\text{O}$ , although the  $\text{NO}_x$  conversion could restore to a certain extent, but still lower than the original value, indicating an irreversible inhibition effect by  $\text{SO}_2$  and  $\text{H}_2\text{O}$ . Fig. 6(c) shows that the activity loss for  $\text{Cu}_{0.5}\text{Mg}_{1.5}\text{Mn}_{0.5}\text{Al}_{0.5}\text{O}_x$ ,  $\text{Mg}_2\text{Mn}_{0.5}\text{Al}_{0.5}\text{O}_x$ ,  $\text{Cu}_2\text{Mn}_{0.5}\text{Al}_{0.5}\text{O}_x$ , and  $\text{Mn}/\gamma\text{-Al}_2\text{O}_3$  was about 10.9% (96.6–85.7%), 14.7% (93.2–78.5%), 20.5% (91.2–70.7%), and 18.7% (59.3–40.6%), respectively. This result also suggested that  $\text{Cu}_{0.5}\text{Mg}_{1.5}\text{Mn}_{0.5}\text{Al}_{0.5}\text{O}_x$  catalyst was less inhibited by  $\text{SO}_2$  and  $\text{H}_2\text{O}$  due to the introduction of Mg.

We have demonstrated that the better  $\text{SO}_2$  and  $\text{H}_2\text{O}$  tolerance of  $\text{Cu}_{0.5}\text{Mg}_{1.5}\text{Mn}_{0.5}\text{Al}_{0.5}\text{O}_x$  catalyst may be mainly due to the introduction of Mg. For Mn-based catalysts, the formation of  $\text{Mn}_2(\text{SO}_4)_3$  and  $\text{Mn}(\text{SO}_4)_2$  could affect its redox properties, and thus inhibit nitrate formation and adsorption [50]. The Mg in  $\text{Cu}_{0.5}\text{Mg}_{1.5}\text{Mn}_{0.5}\text{Al}_{0.5}\text{O}_x$  catalyst can alleviate the competitive adsorption between  $\text{SO}_2$ ,  $\text{H}_2\text{O}$  and the reactants. Once Mg was added, the formation of  $\text{Mn}_2(\text{SO}_4)_3$  and  $\text{Mn}(\text{SO}_4)_2$  can be inhibited, and the deposition of  $(\text{NH}_4)_2\text{SO}_4$  and  $\text{NH}_4\text{HSO}_4$  could be significantly inhibited. Therefore, the newly designed  $\text{Cu}_{0.5}\text{Mg}_{1.5}\text{Mn}_{0.5}\text{Al}_{0.5}\text{O}_x$  catalyst possesses markedly improved resistance to both respective and simultaneous  $\text{H}_2\text{O}$  and  $\text{SO}_2$  poisoning.

Considering the fact that the deactivation of catalysts can not be completely prevented, the regenerability of deactivated catalysts is also very important. In this study, thermal regeneration was

selected to recover the catalytic activity of all deactivated catalysts. The deactivated catalyst was a vulcanized catalyst obtained after the above sulfur resistance test with 100 ppm SO<sub>2</sub>. Fig. 6(d) shows the NO<sub>x</sub> conversion of the deactivated catalysts after thermal regeneration. The NO<sub>x</sub> conversion at 150 °C on fresh Cu<sub>0.5</sub>Mg<sub>1.5</sub>Mn<sub>0.5</sub>Al<sub>0.5</sub>O<sub>x</sub>, Mg<sub>2</sub>Mn<sub>0.5</sub>Al<sub>0.5</sub>O<sub>x</sub>, Cu<sub>2</sub>Mn<sub>0.5</sub>Al<sub>0.5</sub>O<sub>x</sub>, and Mn/γ-Al<sub>2</sub>O<sub>3</sub> was 96.67%, 93.2%, 91.2%, and 59.3%, respectively. With 100 ppm SO<sub>2</sub>, the NO<sub>x</sub> conversion for Cu<sub>0.5</sub>Mg<sub>1.5</sub>Mn<sub>0.5</sub>Al<sub>0.5</sub>O<sub>x</sub>, Mg<sub>2</sub>Mn<sub>0.5</sub>Al<sub>0.5</sub>O<sub>x</sub>, Cu<sub>2</sub>Mn<sub>0.5</sub>Al<sub>0.5</sub>O<sub>x</sub>, and Mn/γ-Al<sub>2</sub>O<sub>3</sub> catalysts became 64.9%, 43.9%, 31.8%, and 21.8%, respectively, after 5 h. After thermal regeneration, the NO<sub>x</sub> conversion of Cu<sub>0.5</sub>Mg<sub>1.5</sub>Mn<sub>0.5</sub>Al<sub>0.5</sub>O<sub>x</sub>, Mg<sub>2</sub>Mn<sub>0.5</sub>Al<sub>0.5</sub>O<sub>x</sub>, Cu<sub>2</sub>Mn<sub>0.5</sub>Al<sub>0.5</sub>O<sub>x</sub>, and Mn/γ-Al<sub>2</sub>O<sub>3</sub> was recovered to 88.9%, 83.1, 84.8%, and 48.8%, respectively. These results clearly indicated that Cu<sub>0.5</sub>Mg<sub>1.5</sub>Mn<sub>0.5</sub>Al<sub>0.5</sub>O<sub>x</sub> has much better regenerability and greater potential for practical applications than other control catalysts.

The long-term stabilities of all catalysts with/without 100 ppm SO<sub>2</sub>+5% H<sub>2</sub>O at 150 °C were compared in Fig. 7(a). After 18 h, the NO<sub>x</sub> conversion of Cu<sub>0.5</sub>Mg<sub>1.5</sub>Mn<sub>0.5</sub>Al<sub>0.5</sub>O<sub>x</sub> catalyst only decreased by 6.5% (from 96.7% to 90.2%) in the absence of 100 ppm SO<sub>2</sub>+5% H<sub>2</sub>O. While, the declines in NO<sub>x</sub> conversion for Mg<sub>2</sub>Mn<sub>0.5</sub>Al<sub>0.5</sub>O<sub>x</sub> (9.6%, from 93.3% to 83.7%), Cu<sub>2</sub>Mn<sub>0.5</sub>Al<sub>0.5</sub>O<sub>x</sub> (9.6%, from 91.2% to 81.6%) and Mn/γ-Al<sub>2</sub>O<sub>3</sub> (14.2%, from 67.2% to 53%) were much more significant. The Cu<sub>0.5</sub>Mg<sub>1.5</sub>Mn<sub>0.5</sub>Al<sub>0.5</sub>O<sub>x</sub> catalyst also exhibited good stability even in the presence of 100 ppm SO<sub>2</sub>+5% H<sub>2</sub>O. After 18 h operation, the decline in NO<sub>x</sub> conversion was only 4% (from 68.2% to 64.2%), and the final NO<sub>x</sub> conversion (64.2%) was much higher than that of all other catalysts, 50.7% for Mg<sub>2</sub>Mn<sub>0.5</sub>Al<sub>0.5</sub>O<sub>x</sub>, 35.5% for Cu<sub>2</sub>Mn<sub>0.5</sub>Al<sub>0.5</sub>O<sub>x</sub>, and 12.5% for Mn/γ-Al<sub>2</sub>O<sub>3</sub>. The results suggested that Cu<sub>0.5</sub>Mg<sub>1.5</sub>Mn<sub>0.5</sub>Al<sub>0.5</sub>O<sub>x</sub> catalyst has better stability and is less influenced by SO<sub>2</sub> and H<sub>2</sub>O comparing with other control catalysts.

To clarify the deactivation was due to SO<sub>2</sub>, SO<sub>2</sub>-TPD for Mn/γ-Al<sub>2</sub>O<sub>3</sub>, Cu<sub>2</sub>Mn<sub>0.5</sub>Al<sub>0.5</sub>O<sub>x</sub>, Cu<sub>0.5</sub>Mg<sub>1.5</sub>Mn<sub>0.5</sub>Al<sub>0.5</sub>O<sub>x</sub>, and Mg<sub>2</sub>Mn<sub>0.5</sub>Al<sub>0.5</sub>O<sub>x</sub> was performed after exposure to 5000 ppm SO<sub>2</sub> for 1 h at 150 °C (Fig. 7(b)). Mn/γ-Al<sub>2</sub>O<sub>3</sub> catalyst that deactivated rapidly in the presence of SO<sub>2</sub> showed the largest peak in the SO<sub>2</sub>-TPD spectra. Cu<sub>0.5</sub>Mg<sub>1.5</sub>Mn<sub>0.5</sub>Al<sub>0.5</sub>O<sub>x</sub> and Mg<sub>2</sub>Mn<sub>0.5</sub>Al<sub>0.5</sub>O<sub>x</sub> catalysts showed much weaker SO<sub>2</sub>-TPD peaks than Mn/γ-Al<sub>2</sub>O<sub>3</sub> and Cu<sub>2</sub>Mn<sub>0.5</sub>Al<sub>0.5</sub>O<sub>x</sub> catalysts, indicating

that the addition of Mg may inhibit the reaction between manganese and SO<sub>2</sub>. Particularly Cu<sub>0.5</sub>Mg<sub>1.5</sub>Mn<sub>0.5</sub>Al<sub>0.5</sub>O<sub>x</sub> showed the smallest SO<sub>2</sub>-TPD peak, explaining why it is less effected by the SO<sub>2</sub> poisoning.

### 3.4. In situ DRIFT study on the interaction between SO<sub>2</sub> and NH<sub>3</sub>

NH<sub>3</sub> adsorption is believed to be a key step in NH<sub>3</sub>-SCR reaction. Therefore in order to clarify how SO<sub>2</sub> might impact this process, a comparative study was performed. Fig. 8 shows the DRIFT spectra of Mn/γ-Al<sub>2</sub>O<sub>3</sub>, Cu<sub>2</sub>Mn<sub>0.5</sub>Al<sub>0.5</sub>O<sub>x</sub>, Cu<sub>0.5</sub>Mg<sub>1.5</sub>Mn<sub>0.5</sub>Al<sub>0.5</sub>O<sub>x</sub>, and Mg<sub>2</sub>Mn<sub>0.5</sub>Al<sub>0.5</sub>O<sub>x</sub> after exposure to NH<sub>3</sub>/N<sub>2</sub> and SO<sub>2</sub> co-adsorption with NH<sub>3</sub> at different times. The bands at 3336 and 3347 cm<sup>-1</sup> belong to the N-H stretching region [51]. The bands at 1217, 1154, 1153, 1158, 1297, 1577, 1586, and 1588 cm<sup>-1</sup> belong to NH<sub>3</sub> coordinated to L acids [52, 53]. The bands at 1695 cm<sup>-1</sup> and in the range of 1850–1640 cm<sup>-1</sup> belong to NH<sub>4</sub><sup>+</sup> species on B acids [54]. However, for Cu<sub>0.5</sub>Mg<sub>1.5</sub>Mn<sub>0.5</sub>Al<sub>0.5</sub>O<sub>x</sub>, the intensity of band at 1153 cm<sup>-1</sup> was much stronger than that on other catalysts, indicating a stronger adsorption of NH<sub>3</sub> due to the addition of Cu and Mg. This NH<sub>3</sub>-DRIFT result is consistent with the results of pyridine infrared and NH<sub>3</sub>-TPD, indicating that Cu<sub>0.5</sub>Mg<sub>1.5</sub>Mn<sub>0.5</sub>Al<sub>0.5</sub>O<sub>x</sub> has more Lewis acid sites, and may be one of the reasons for its high activity.

All catalysts were then exposed to both NH<sub>3</sub> and SO<sub>2</sub>. In comparing the band intensities after a 30 minute exposure, the intensity of bands corresponding to NH<sub>3</sub> on L acid sites (about 1153 cm<sup>-1</sup>) and B acid sites (1850–1640 cm<sup>-1</sup>) slightly decreased, compared with only NH<sub>3</sub> exposure. The result indicated that the amount of adsorbed NH<sub>3</sub> on L and B acid sites was reduced. However, the intensity of a band assigned to NH<sub>4</sub><sup>+</sup> species increased, which was interpreted by the formation of new NH<sub>4</sub><sup>+</sup> species. Meanwhile, The emergence of new bands at 1287, 1267, 1281, and 1276 cm<sup>-1</sup> suggested the formation of HSO<sub>4</sub><sup>-</sup> species [55]. These results show that SO<sub>2</sub> does has an impact on NH<sub>3</sub> adsorption, and forms some new NH<sub>4</sub>HSO<sub>4</sub> species. Notably, it is clear that during SO<sub>2</sub> co-adsorption with NH<sub>3</sub>, Cu<sub>0.5</sub>Mg<sub>1.5</sub>Mn<sub>0.5</sub>Al<sub>0.5</sub>O<sub>x</sub> still has more L acid sites and less NH<sub>4</sub>HSO<sub>4</sub> species compared with other catalysts, which was very important for the occurrence of SCR reactions.

Based on the above discussion, the high activity of CuMgMnAlO<sub>x</sub> catalyst for low-temperature



NH<sub>3</sub>-SCR should be attributed to high dispersion of manganese oxides, copper oxide and magnesium oxide with a high SSA, abundance of acid sites, etc. In addition, the introduction of Mg, can increase the amount of acid sites, but also adsorb SO<sub>2</sub>, enhancing the sulfur resistance of the catalyst. Therefore, we propose electrons might transfer between Mn and Cu ions. After introducing Cu, the electron transfer was more active. A redox electron transfer between different ions (from Mn and Cu) through the oxygen bridge as Equation (2), which is probably similar to the electron transfer described previously in literature [56-58]. Thus, we proposed a redox cycle for the low-temperature NH<sub>3</sub>-SCR over this novel CuMgMnAlO<sub>x</sub> catalyst, as described in Fig. 9.



#### 4. Conclusions

A novel NH<sub>3</sub>-SCR catalyst with the chemical composition of Cu<sub>0.5</sub>Mg<sub>1.5</sub>Mn<sub>0.5</sub>Al<sub>0.5</sub>O<sub>x</sub> was designed and obtained upon calcination of the Cu<sub>0.5</sub>Mg<sub>1.5</sub>Mn<sub>0.5</sub>Al<sub>0.5</sub>-CO<sub>3</sub> LDH precursor. XRD, FTIR, SEM, and HR-TEM analyses demonstrated the successful synthesis of a series of “flower-like” LDHs, which are good precursors for the fabrication of highly dispersed Cu<sub>w</sub>Mg<sub>2-w</sub>Mn<sub>y</sub>Al<sub>1-y</sub>O<sub>x</sub> mixed oxide catalysts. The best catalyst Cu<sub>0.5</sub>Mg<sub>1.5</sub>Mn<sub>0.5</sub>Al<sub>0.5</sub>O<sub>x</sub> possessed a very high NO<sub>x</sub> removal efficiency of 96.6% at 150 °C, which is much higher than that of Mn/γ-Al<sub>2</sub>O<sub>3</sub> catalyst (59.3%). XRD and XPS analyses indicated that the Cu<sub>0.5</sub>Mg<sub>1.5</sub>Mn<sub>0.5</sub>Al<sub>0.5</sub>O<sub>x</sub> catalyst mainly contains well dispersed MnO<sub>2</sub> and CuO nanoparticles, which are the main active components. In addition, the high concentrations of Mn<sup>4+</sup> and Cu<sup>2+</sup> should also be partly responsible for the good performance of Cu<sub>0.5</sub>Mg<sub>1.5</sub>Mn<sub>0.5</sub>Al<sub>0.5</sub>O<sub>x</sub> catalyst. ESR analysis demonstrated that the Cu<sub>0.5</sub>Mg<sub>1.5</sub>Mn<sub>0.5</sub>Al<sub>0.5</sub>O<sub>x</sub> possesses oxygen vacancies on its surface while the Mn/γ-Al<sub>2</sub>O<sub>3</sub> catalyst did not. NH<sub>3</sub>-TPD, Py-FTIR, in situ DRIFT, and H<sub>2</sub>-TPR analyses indicated that Cu<sub>0.5</sub>Mg<sub>1.5</sub>Mn<sub>0.5</sub>Al<sub>0.5</sub>O<sub>x</sub> possesses more acid sites and higher reducibility than the control catalyst Mn/γ-Al<sub>2</sub>O<sub>3</sub>. Cu<sub>0.5</sub>Mg<sub>1.5</sub>Mn<sub>0.5</sub>Al<sub>0.5</sub>O<sub>x</sub> catalyst was also demonstrated to possess much better SO<sub>2</sub> and H<sub>2</sub>O resistance than the control catalyst Mn/γ-Al<sub>2</sub>O<sub>3</sub>. The regeneration studies of deactivated catalysts by thermal treatment at high temperatures indicated that the NO<sub>x</sub> conversion

of  $\text{Cu}_{0.5}\text{Mg}_{1.5}\text{Mn}_{0.5}\text{Al}_{0.5}\text{O}_x$  could be recovered to 88.9%, which is only slightly lower than its initial value (96.7%).

## Acknowledgements

This work was supported by the National Natural Science Foundation of China (51622801, 51572029), and the Beijing Excellent Young Scholar (2015000026833ZK11).

## References

- [1] J.A. Sullivan, J.A. Doherty,  $\text{NH}_3$  and urea in the selective catalytic reduction of  $\text{NO}_x$  over oxide-supported copper catalysts, *Appl. Catal. B: Environ.* 55 (2005) 185-194.
- [2] J.M. García-Cortés, J. Pérez-Ramírez, M.J. Illán-Gómez, F. Kapteijin, J.A. Moulijn, C.S.M. de Lecea, Comparative study of Pt-based catalysts on different supports in the low-temperature de- $\text{NO}_x$ -SCR with propene, *Appl. Catal. B: Environ.* 30 (2001) 399-408.
- [3] W.S. Kijlstra, D.S. Brands, E.K. Poels, A. Blik, Mechanism of the Selective Catalytic Reduction of NO by  $\text{NH}_3$  over  $\text{MnO}_x/\text{Al}_2\text{O}_3$ , *J. catal.* 171 (1997) 208-218.
- [4] M. Richter, A. Trunschke, U. Bentrup, K.W. Brzezinka, E. Schreier, M. Schneider, M.-M. Pohl, R. Fricke, Selective catalytic reduction of nitric oxide by ammonia over egg-shell  $\text{MnO}_x/\text{NaY}$  composite catalysts, *J. catal.* 206 (2002) 98-113.
- [5] G. Qi, R.T. Yang, R. Chang,  $\text{MnO}_x$ - $\text{CeO}_2$  mixed oxides prepared by co-precipitation for selective catalytic reduction of NO with  $\text{NH}_3$  at low temperatures, *Appl. Catal. B: Environ.* 51 (2004) 93-106.
- [6] G. Qi, R.T. Yang, Low-temperature selective catalytic reduction of NO with  $\text{NH}_3$  over iron and manganese oxides supported on titania, *Appl. Catal. B: Environ.* 44 (2003) 217-225.
- [7] G. Qi, R.T. Yang, R. Chang, Low-temperature SCR of NO with  $\text{NH}_3$  over USY-supported manganese oxide-based catalysts, *Catal. Lett.* 87 (2003) 67-71.
- [8] G. Qi, R.T. Yang, Characterization and FTIR studies of  $\text{MnO}_x$ - $\text{CeO}_2$  catalyst for low-temperature selective catalytic reduction of NO with  $\text{NH}_3$ , *J. Phys. Chem. B* 108 (2004) 15738-15747.
- [9] G. Marbán, T. Valdés-Solís, A.B. Fuertes, Mechanism of low-temperature selective catalytic reduction of NO with  $\text{NH}_3$  over carbon-supported  $\text{Mn}_3\text{O}_4$ : Role of surface  $\text{NH}_3$  species: SCR mechanism, *J. catal.* 226 (2004) 138-155.
- [10] M. Wallin, S. Forser, P. Thormählen, M. Skoglundh, Screening of  $\text{TiO}_2$ -supported catalysts for selective  $\text{NO}_x$  reduction with ammonia, *Ind. Eng. Chem. Res.* 43 (2004) 7723-7731.
- [11] H.Y. Huang, R.T. Yang, Removal of NO by reversible adsorption on Fe-Mn based transition metal oxides, *Langmuir* 17 (2001) 4997-5003.
- [12] Q. Wang, X. Zhang, C.J. Wang, J. Zhu, Z. Guo, D. O'Hare, Polypropylene/layered double hydroxide nanocomposites, *J. Mater. Chem.* 22 (2012) 19113-19121.
- [13] Y. Gao, Z. Zhang, J. Wu, X. Yi, A. Zheng, A. Umar, D. O'Hare, Q. Wang, Comprehensive investigation of  $\text{CO}_2$  adsorption on Mg-Al- $\text{CO}_3$  LDH-derived mixed metal oxides, *J. Mater. Chem. A* 1 (2013) 12782-12790.
- [14] Y. Zhao, G. Chen, T. Bian, C. Zhou, G.I. Waterhouse, L.Z. Wu, C.H. Tung, L.J. Smith, D. O'Hare, T. Zhang, Defect-Rich Ultrathin ZnAl-Layered Double Hydroxide Nanosheets for Efficient

Photoreduction of CO<sub>2</sub> to CO with Water, *Adv. Mater.* 27 (2015) 7824-7831.

[15] J. Wang, Y. Yang, L. Jia, N. Yang, Q. Guan, L. Huang, A. Umar, Q. Wang, P. Ning, The Influence of the Charge Compensating Anions of Layered Double Hydroxides (LDHs) in LDH-NS/Graphene Oxide Nanohybrid for CO<sub>2</sub> Capture, *J. nanosci. nanotechnol.* 18 (2018) 2956-2964.

[16] C. Gennequin, T. Barakat, H.L. Tidahy, R. Cousin, J.F. Lamonier, A. Aboukaïs, S. Siffert, Use and observation of the hydrotalcite “memory effect” for VOC oxidation, *Catal. Today* 157 (2010) 191-197.

[17] Y. Zhao, X. Jia, G. Chen, L. Shang, G.I. Waterhouse, L.Z. Wu, C.H. Tung, D. O'Hare, T. Zhang, Ultrafine NiO nanosheets stabilized by TiO<sub>2</sub> from monolayer NiTi-LDH precursors: an active water oxidation electrocatalyst, *J. Am. Chem. Soc.* 138 (2016) 6517-6524.

[18] G. Xie, Z. Liu, Z. Zhu, Q. Liu, J. Ge, Z. Huang, Simultaneous removal of SO<sub>2</sub> and NO<sub>x</sub> from flue gas using a CuO/Al<sub>2</sub>O<sub>3</sub> catalyst sorbent: II. Promotion of SCR activity by SO<sub>2</sub> at high temperatures, *J. Catal.* 224 (2004) 42-49.

[19] Y. Bao, C. Huang, L. Chen, Y. Zhang, L. Liang, J. Wen, M. Fu, J. Wu, D. Ye, Highly efficient Cu/anatase TiO<sub>2</sub> {001}-nanosheets catalysts for methanol synthesis from CO<sub>2</sub>, *J. Energ. Chem.* 27 (2018) 381-388.

[20] W. Gao, T. Zhou, Y. Gao, B. Louis, D. O'Hare, Q. Wang, Molten salts-modified MgO-based adsorbents for intermediate-temperature CO<sub>2</sub> capture: a review, *J. Energ. Chem.* 26 (2017) 830-838.

[21] Q. Wang, Y. Gao, J. Luo, Z. Zhong, A. Borgna, Z. Guo, D. O'Hare, Synthesis of nano-sized spherical Mg<sub>3</sub>Al-CO<sub>3</sub> layered double hydroxide as a high-temperature CO<sub>2</sub> adsorbent, *RSC Advances* 3 (2013) 3414-3420.

[22] Q. Wang, H.H. Tay, D.J.W. Ng, L. Chen, Y. Liu, J. Chang, Z. Zhong, J. Luo, A. Borgna, The Effect of Trivalent Cations on the Performance of Mg-M-CO<sub>3</sub> Layered Double Hydroxides for High-Temperature CO<sub>2</sub> Capture, *ChemSusChem* 3 (2010) 965-973.

[23] M. Yu, C. Li, G. Zeng, Y. Zhou, X. Zhang, The selective catalytic reduction of NO with NH<sub>3</sub> over a novel Ce-Sn-Ti mixed oxides catalyst: Promotional effect of SnO<sub>2</sub>, *Appl. Surf. Sci.* 342 (2015) 174-182.

[24] B. Jiang, Y. Liu, Z. Wu, Low-temperature selective catalytic reduction of NO on MnO<sub>x</sub>/TiO<sub>2</sub> prepared by different methods, *J. Hazard. Mater.* 162 (2009) 1249-1254.

[25] F. Liu, H. He, Structure-Activity Relationship of Iron Titanate Catalysts in the Selective Catalytic Reduction of NO<sub>x</sub> with NH<sub>3</sub>, *J. Phys. Chem. C* 114 (2010) 16929-16936.

[26] L. Zhang, L. Li, Y. Zhang, Y. Zhao, J. Li, Nickel catalysts supported on MgO with different specific surface area for carbon dioxide reforming of methane, *J. Energ. Chem.* 23 (2014) 66-72.

[27] Q. Jia, S. Shan, L. Jiang, Y. Wang, D. Li, Synergistic antimicrobial effects of polyaniline combined with silver nanoparticles, *J. Appl. Polym. Sci.* 125 (2012) 3560-3566.

[28] A. Zhou, D. Yu, L. Yang, Z. Sheng, Combined effects Na and SO<sub>2</sub> in flue gas on Mn-Ce/TiO<sub>2</sub> catalyst for low temperature selective catalytic reduction of NO by NH<sub>3</sub> simulated by Na<sub>2</sub>SO<sub>4</sub> doping, *Appl. Surf. Sci.* 378 (2016) 167-173.

[29] A.S. Reddy, C.S. Gopinath, S. Chilukuri, Selective ortho-methylation of phenol with methanol over copper manganese mixed-oxide spinel catalysts, *J. Catal.* 243 (2006) 278-291.

[30] F. Kapteijn, A.D. Vanlangeveld, J.A. Moulijn, A. Andreini, M.A. Vuurman, A.M. Turek, J.-M. Jehng, I.E. Wachs, Alumina-supported manganese oxide catalysts: I. Characterization: effect of precursor and loading, *J. Catal.* 150 (1994) 94-104.

[31] X. Tang, J. Li, L. Sun, J. Hao, Origination of N<sub>2</sub>O from NO reduction by NH<sub>3</sub> over β-MnO<sub>2</sub> and α-Mn<sub>2</sub>O<sub>3</sub>, *Appl. Catal. B: Environ.* 99 (2010) 156-162.

[32] Y. Wu, Y. Lu, C. Song, Z. Ma, S. Xing, Y. Gao, A novel redox-precipitation method for the

preparation of  $\alpha$ -MnO<sub>2</sub> with a high surface Mn<sup>4+</sup> concentration and its activity toward complete catalytic oxidation of o-xylene, *Catal. Today* 201 (2013) 32-39.

[33] C. Fang, D. Zhang, S. Cai, L. Zhang, L. Huang, H. Li, P. Maitarad, L. Shi, R. Gao, J. Zhang, Low-temperature selective catalytic reduction of NO with NH<sub>3</sub> over nanoflaky MnO<sub>x</sub> on carbon nanotubes in situ prepared via a chemical bath deposition route, *Nanoscale* 5 (2013) 9199-9207.

[34] L. Chen, J. Li, M. Ge, The poisoning effect of alkali metals doping over nano V<sub>2</sub>O<sub>5</sub>-WO<sub>3</sub>/TiO<sub>2</sub> catalysts on selective catalytic reduction of NO<sub>x</sub> by NH<sub>3</sub>, *Chem. Eng. J.* 170 (2011) 531-537.

[35] Q. Li, H. Yang, F. Qiu, X. Zhang, Promotional effects of carbon nanotubes on V<sub>2</sub>O<sub>5</sub>/TiO<sub>2</sub> for NO<sub>x</sub> removal, *J. hazard. mater.* 192 (2011) 915-921.

[36] J. Xue, X. Wang, G. Qi, J. Wang, M. Shen, W. Li, Characterization of copper species over Cu/SAPO-34 in selective catalytic reduction of NO<sub>x</sub> with ammonia: Relationships between active Cu sites and de-NO<sub>x</sub> performance at low temperature, *J. Catal.* 297 (2013) 56-64.

[37] D. Yuan, X. Li, Q. Zhao, J. Zhao, M. Tadé, S. Liu, A novel CuTi-containing catalyst derived from hydrotalcite-like compounds for selective catalytic reduction of NO with C<sub>3</sub>H<sub>6</sub> under lean-burn conditions, *J. catal.* 309 (2014) 268-279.

[38] M.I. Zaki, M.A. Hasan, F.A. Al-Sagheer, L. Pasupulety, In situ FTIR spectra of pyridine adsorbed on SiO<sub>2</sub>-Al<sub>2</sub>O<sub>3</sub>, TiO<sub>2</sub>, ZrO<sub>2</sub> and CeO<sub>2</sub>: general considerations for the identification of acid sites on surfaces of finely divided metal oxides, *Colloid. Surf. A* 190 (2001) 261-274.

[39] D.A. Peña, B.S. Uphade, P.G. Smirniotis, TiO<sub>2</sub>-supported metal oxide catalysts for low-temperature selective catalytic reduction of NO with NH<sub>3</sub>: I. Evaluation and characterization of first row transition metals, *J. Catal.* 221 (2004) 421-431.

[40] D. Yuan, X. Li, Q. Zhao, J. Zhao, S. Liu, M. Tadé, Effect of surface Lewis acidity on selective catalytic reduction of NO by C<sub>3</sub>H<sub>6</sub> over calcined hydrotalcite, *Appl. Catal. A: Gen.* 451 (2013) 176-183.

[41] P. Kalita, N.M. Gupta, R. Kumar, Synergistic role of acid sites in the Ce-enhanced activity of mesoporous Ce-Al-MCM-41 catalysts in alkylation reactions: FTIR and TPD-ammonia studies, *J. Catal.* 245 (2007) 338-347.

[42] N. Li, A. Wang, M. Zheng, X. Wang, R. Cheng, T. Zhang, Probing into the catalytic nature of Co/sulfated zirconia for selective reduction of NO with methane, *J. Catal.* 225 (2004) 307-315.

[43] J. Zhu, F. Gao, L. Dong, W. Yu, L. Qi, Z. Wang, L. Dong, Y. Chen, Studies on surface structure of M<sub>x</sub>O<sub>y</sub>/MoO<sub>3</sub>/CeO<sub>2</sub> system (M= Ni, Cu, Fe) and its influence on SCR of NO by NH<sub>3</sub>, *Appl. Catal. B: Environ.* 95 (2010) 144-152.

[44] J. Li, Q. Jia, J. Zhu, M. Zheng, Interfacial polymerization of morphologically modified polyaniline: from hollow microspheres to nanowires, *Polym. int.* 57 (2008) 337-341.

[45] M. Kang, E.D. Park, J.M. Kim, J.E. Yie, Cu-Mn mixed oxides for low temperature NO reduction with NH<sub>3</sub>, *Catal. Today* 111 (2006) 236-241.

[46] Q. Yan, Y. Nie, R. Yang, Y. Cui, D. O'Hare, Q. Wang, Highly dispersed Cu<sub>y</sub>AlO<sub>x</sub> mixed oxides as superior low-temperature alkali metal and SO<sub>2</sub> resistant NH<sub>3</sub>-SCR catalysts, *Appl. Catal. A: Gen.* 538 (2017) 37-50.

[47] J. Qi, Y. Sun, Z. Xie, M. Collins, H. Du, T. Xiong, Development of Cu foam-based Ni catalyst for solar thermal reforming of methane with carbon dioxide, *J. Energ. Chem.* 24 (2015) 786-793.

[48] S. Zhang, Q. Zhong, Promotional effect of WO<sub>3</sub> on O<sub>2</sub><sup>-</sup> over V<sub>2</sub>O<sub>5</sub>/TiO<sub>2</sub> catalyst for selective catalytic reduction of NO with NH<sub>3</sub>, *J. Mol. Catal. A: Chem.* 373 (2013) 108-113.

[49] Z. Liu, Y. Yi, J. Li, S.I. Woo, B. Wang, X. Cao, Z. Li, A superior catalyst with dual redox cycles for the selective reduction of NO<sub>x</sub> by ammonia, *Chem. Commun.* 49 (2013) 7726-7728.

[50] L. Wei, S. Cui, H. Guo, X. Ma, L. Zhang, DRIFT and DFT study of cerium addition on SO<sub>2</sub> of

- Manganese-based Catalysts for low temperature SCR, *J. Mol. Catal. A: Chem.* 421 (2016) 102-108.
- [51] S. Sayan, M. Kantcheva, S. Suzer, D.O. Uner, FTIR characterization of Ru/SiO<sub>2</sub> catalyst for ammonia synthesis, *J. Mol. Struct.* 480 (1999) 241-245.
- [52] L. Zhang, J. Pierce, V.L. Leung, D. Wang, W.S. Epling, Characterization of Ceria's Interaction with NO<sub>x</sub> and NH<sub>3</sub>, *J. Phys. Chem. C* 117 (2013) 8282-8289.
- [53] T. Jin, T. Yamaguchi, K. Tanabe, Mechanism of acidity generation on sulfur-promoted metal oxides, *J. Phys. Chem.* 90 (1986) 4794-4796.
- [54] S.D. Lin, A.C. Gluhoi, B.E. Nieuwenhuys, Ammonia oxidation over Au/MO<sub>x</sub>/γ-Al<sub>2</sub>O<sub>3</sub>-activity, selectivity and FTIR measurements, *Catal. Today* 90 (2004) 3-14.
- [55] L. Zhang, L. Li, Y. Cao, X. Yao, C. Ge, F. Gao, Y. Deng, C. Tang, L. Dong, Getting insight into the influence of SO<sub>2</sub> on TiO<sub>2</sub>/CeO<sub>2</sub> for the selective catalytic reduction of NO by NH<sub>3</sub>, *Appl. Catal. B: Environ.* 165 (2015) 589-598.
- [56] F.C. Buciuman, F. Patcas, T. Hahn, A spillover approach to oxidation catalysis over copper and manganese mixed oxides, *Chem. Eng. Process.* 38 (1999) 563-569.
- [57] Z. Chen, Q. Yang, H. Li, X. Li, L. Wang, S.C. Tsang, Cr-MnO<sub>x</sub> mixed-oxide catalysts for selective catalytic reduction of NO<sub>x</sub> with NH<sub>3</sub> at low temperature, *J. Catal.* 276 (2010) 56-65.
- [58] S. Vepřek, D.L. Cocke, S. Kehl, H.R. Oswald, Mechanism of the deactivation of Hopcalite catalysts studied by XPS, ISS, and other techniques, *J. Catal.* 100 (1986) 250-263.

**Table 1** SSA, pore size, and pore volume of Mn/ $\gamma$ -Al<sub>2</sub>O<sub>3</sub> and Cu<sub>w</sub>Mg<sub>2-w</sub>Mn<sub>0.5</sub>Al<sub>0.5</sub>O<sub>x</sub> catalysts.

Catalysts	BET SSA (m <sup>2</sup> /g)	BJH Pore size (Å)	BJH pore volume (cm <sup>3</sup> /g)
Mn/ $\gamma$ -Al <sub>2</sub> O <sub>3</sub>	135.5	54.9	0.37
Cu <sub>2</sub> Mn <sub>0.5</sub> Al <sub>0.5</sub> O <sub>x</sub>	136.4	150.9	1.03
Cu <sub>1.5</sub> Mg <sub>0.5</sub> Mn <sub>0.5</sub> Al <sub>0.5</sub> O <sub>x</sub>	157.1	188.0	1.47
Cu <sub>1</sub> Mg <sub>1</sub> Mn <sub>0.5</sub> Al <sub>0.5</sub> O <sub>x</sub>	188.9	143.3	1.35
Cu <sub>0.5</sub> Mg <sub>1.5</sub> Mn <sub>0.5</sub> Al <sub>0.5</sub> O <sub>x</sub>	228.7	146.9	1.68
Mg <sub>2</sub> Mn <sub>0.5</sub> Al <sub>0.5</sub> O <sub>x</sub>	220.3	84.7	0.95

**Table 2** The surface chemical compositions of  $\text{Mg}_2\text{Mn}_{0.5}\text{Al}_{0.5}\text{O}_x$ ,  $\text{Cu}_{0.5}\text{Mg}_{1.5}\text{Mn}_{0.5}\text{Al}_{0.5}\text{O}_x$ ,  $\text{Cu}_2\text{Mn}_{0.5}\text{Al}_{0.5}\text{O}_x$ , and  $\text{Mn}/\gamma\text{-Al}_2\text{O}_3$  catalysts determined by XPS analyses.

Catalysts	$\text{Mn}^{4+}$ $/(\text{Mn}^{4+}+\text{Mn}^{3+})$ (%)	$\text{Cu}^{2+}$ $/(\text{Cu}^{2+}+\text{Cu}^{1+})$ (%)	$\text{O}_\beta$ $/(\text{O}_\beta+\text{O}_a)$ (%)
$\text{Mg}_2\text{Mn}_{0.5}\text{Al}_{0.5}\text{O}_x$	78.5	-	51.6
$\text{Cu}_{0.5}\text{Mg}_{1.5}\text{Mn}_{0.5}\text{Al}_{0.5}\text{O}_x$	90.1	93	59.8
$\text{Cu}_2\text{Mn}_{0.5}\text{Al}_{0.5}\text{O}_x$	67.7	91	65.3
$\text{Mn}/\gamma\text{-Al}_2\text{O}_3$	39.5	-	37.3

**Table 3** The  $\text{Cu}^{2+}$  and/or  $\text{Mn}^{4+}$  content and TOFs of  $\text{Mg}_2\text{Mn}_{0.5}\text{Al}_{0.5}\text{O}_x$ ,  $\text{Cu}_{0.5}\text{Mg}_{1.5}\text{Mn}_{0.5}\text{Al}_{0.5}\text{O}_x$ ,  $\text{Cu}_2\text{Mn}_{0.5}\text{Al}_{0.5}\text{O}_x$ , and  $\text{Mn}/\gamma\text{-Al}_2\text{O}_3$  catalysts.

Catalysts	$\text{Cu}^{2+\text{a}}$ (wt.%)	$\text{Mn}^{4+\text{a}}$ (wt.%)	$\text{TOF}^{\text{b}} \times 10^{-4} (\text{s}^{-1})$					
			100 °C		150 °C		200 °C	
			$\text{Cu}^{2+}$	$\text{Mn}^{4+}$	$\text{Cu}^{2+}$	$\text{Mn}^{4+}$	$\text{Cu}^{2+}$	$\text{Mn}^{4+}$
$\text{Mn}/\gamma\text{-Al}_2\text{O}_3$	-	1.32	-	7.4	-	12.2	-	13.8
$\text{Cu}_2\text{Mn}_{0.5}\text{Al}_{0.5}\text{O}_x$	53.1	8.2	0.31	1.7	0.54	3	0.49	2.78
$\text{Cu}_{0.5}\text{Mg}_{1.5}\text{Mn}_{0.5}\text{Al}_{0.5}\text{O}_x$	18.2	17.85	1.6	1.4	1.68	1.48	1.61	1.41
$\text{Mg}_2\text{Mn}_{0.5}\text{Al}_{0.5}\text{O}_x$	-	15.95	-	0.92	-	1.6	-	1.38

a Total  $\text{Cu}^{2+}$  or  $\text{Mn}^{4+}$  content analyzed by ICP and XPS.

b TOFs for  $\text{NO}_x$  reaction based on total  $\text{Cu}^{2+}$  or  $\text{Mn}^{4+}$  content.



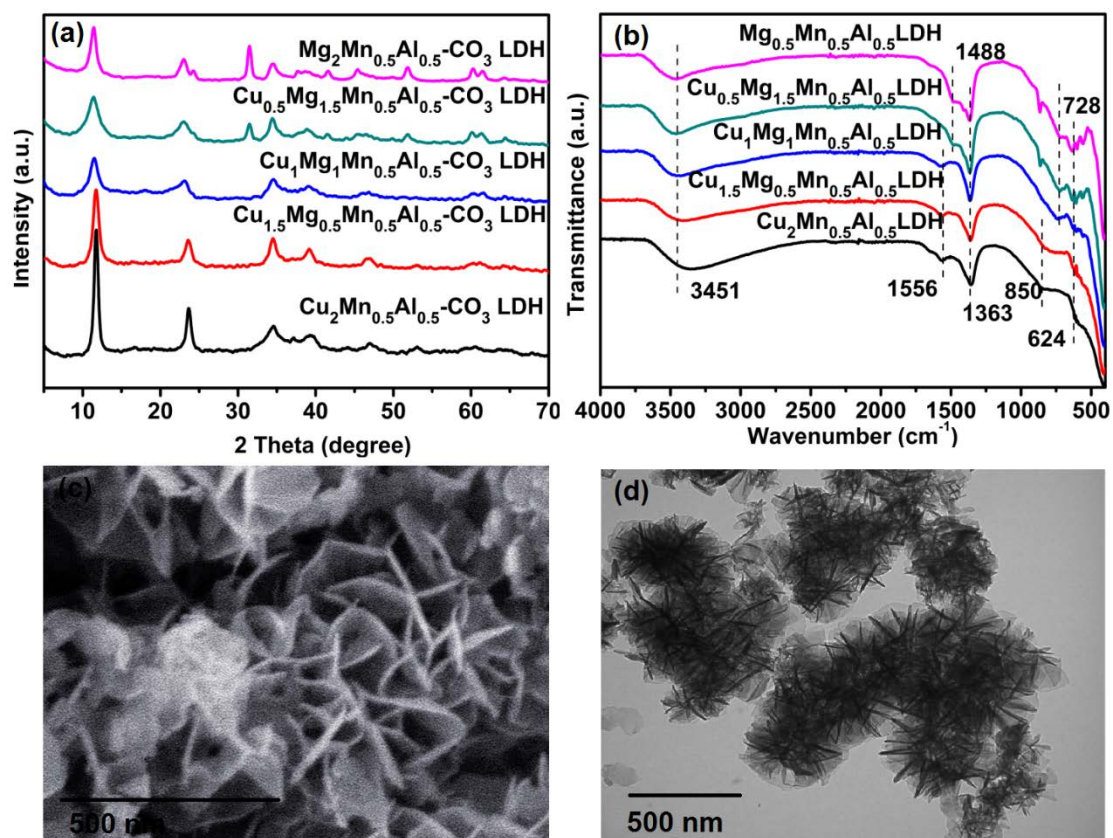


**Fig. 1.** (a) XRD patterns and (b) FTIR spectra of  $\text{Cu}_{2-w}\text{Mg}_w\text{Mn}_{0.5}\text{Al}_{0.5}\text{-CO}_3$  LDHs, (c) SEM and (d) TEM image of  $\text{Cu}_{0.5}\text{Mg}_{1.5}\text{Mn}_{0.5}\text{Al}_{0.5}\text{-CO}_3$  LDH.

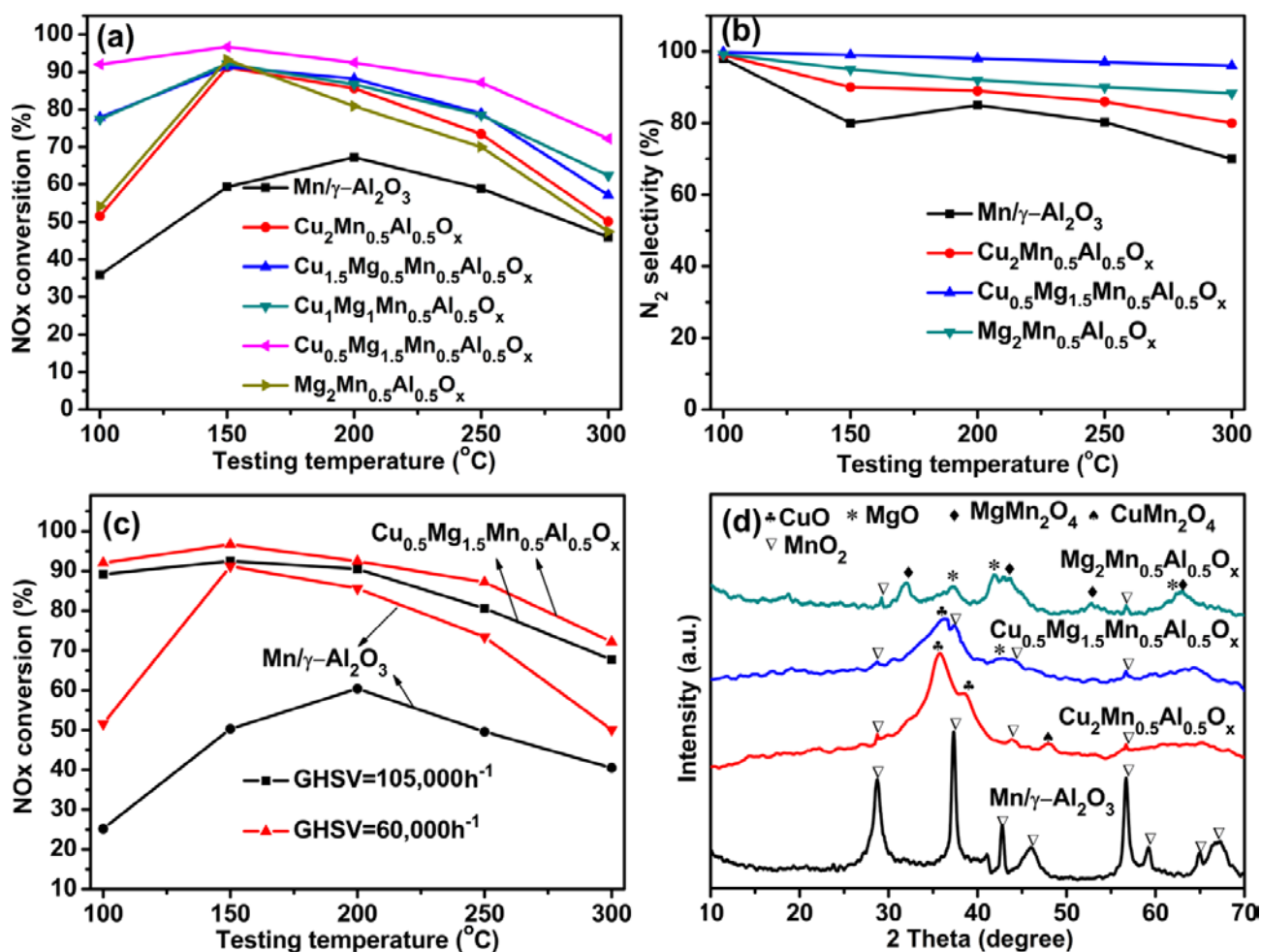


**Fig. 2.** (a) The NO<sub>x</sub> conversions of catalysts, (b) N<sub>2</sub> selectivity of catalysts, (c) NO<sub>x</sub> conversion over Mn/γ-Al<sub>2</sub>O<sub>3</sub> and Cu<sub>0.5</sub>Mg<sub>1.5</sub>Mn<sub>0.5</sub>Al<sub>0.5</sub>O<sub>x</sub> catalysts under different GHSVs (60,000 h<sup>-1</sup> and 105,000 h<sup>-1</sup>), and (d) The XRD patterns of catalysts. Reaction conditions: [NO<sub>x</sub>] = [NH<sub>3</sub>] = 500 ppm, [O<sub>2</sub>] = 5%, balance Ar, total flow rate = 200 mL/min, GHSV=60,000 h<sup>-1</sup>, catalyst 0.15 g.

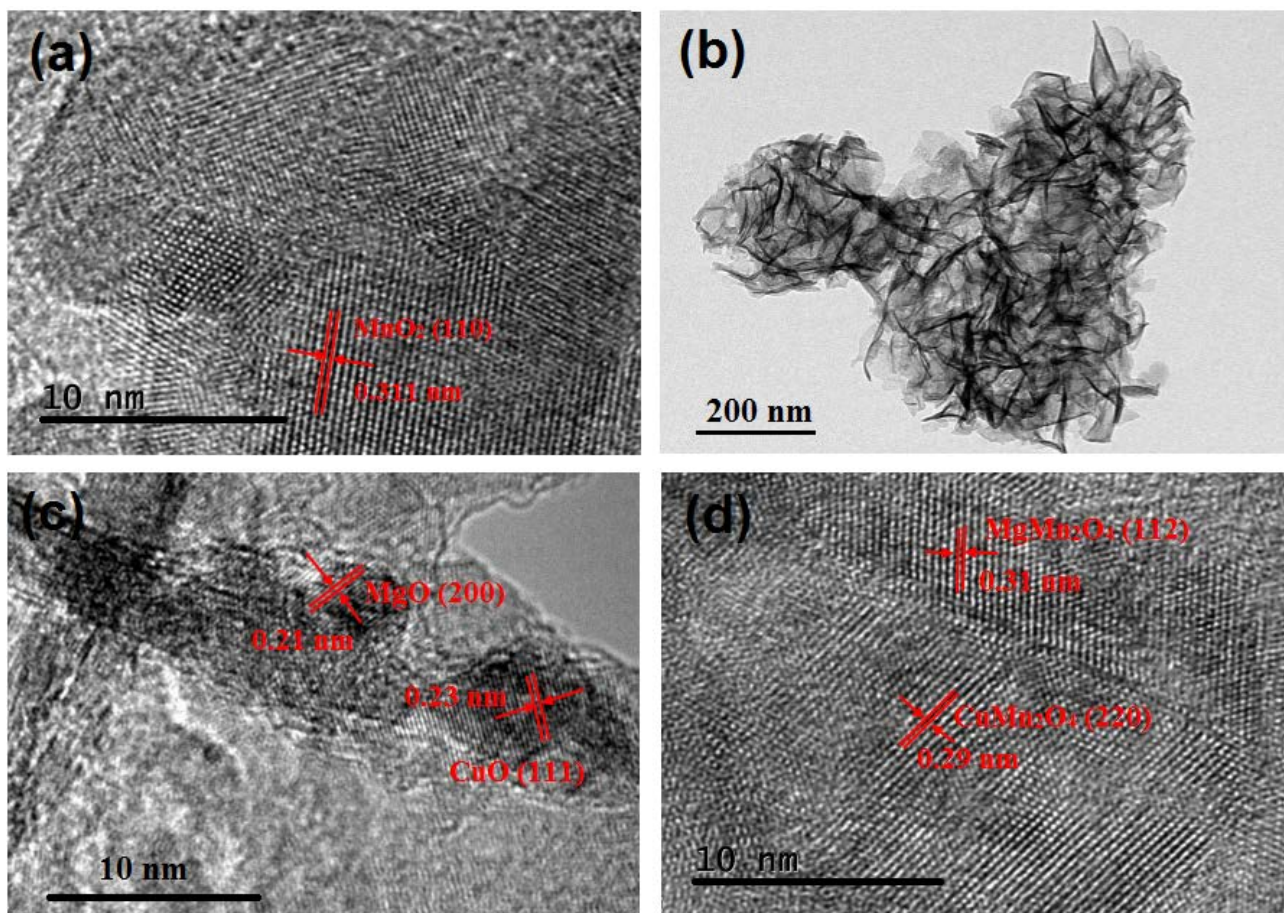


**Fig. 3.** (a) The HR-TEM images of Mn/γ-Al<sub>2</sub>O<sub>3</sub> calcined at 400 °C, (b, c, d) The HR-TEM images of Cu<sub>0.5</sub>Mg<sub>1.5</sub>Mn<sub>0.5</sub>Al<sub>0.5</sub>O<sub>x</sub> calcined at 400 °C.

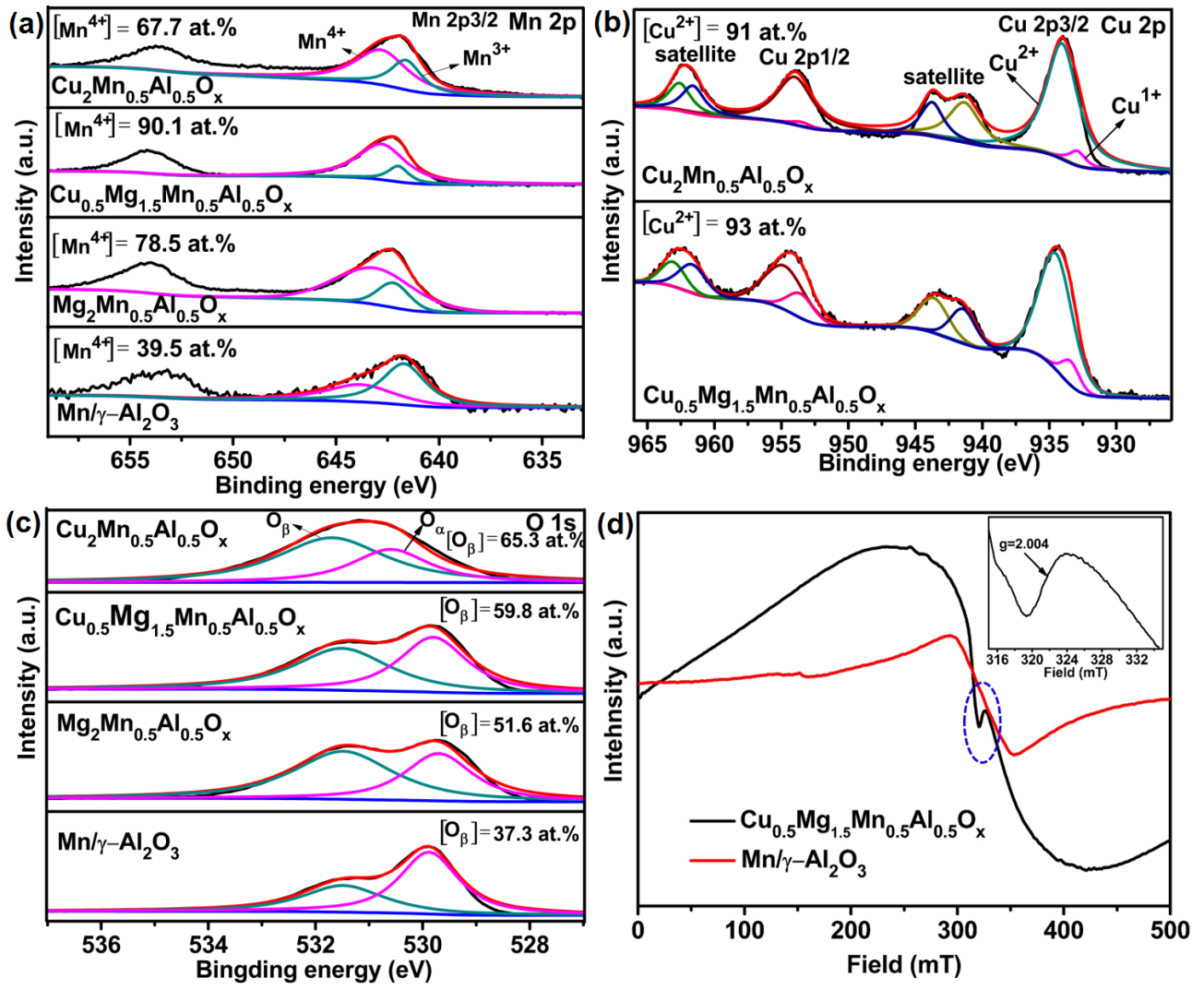


**Fig. 4.** XPS results of (a) Mn 2p, (b) Cu 2p, (c) O 1s over  $\text{Cu}_2\text{Mn}_{0.5}\text{Al}_{0.5}\text{O}_x$ ,  $\text{Cu}_{0.5}\text{Mg}_{1.5}\text{Mn}_{0.5}\text{Al}_{0.5}\text{O}_x$ ,  $\text{Mg}_2\text{Mn}_{0.5}\text{Al}_{0.5}\text{O}_x$ , and  $\text{Mn}/\gamma\text{-Al}_2\text{O}_3$ , and (d) ESR spectra for  $\text{Cu}_{0.5}\text{Mg}_{1.5}\text{Mn}_{0.5}\text{Al}_{0.5}\text{O}_x$ , and  $\text{Mn}/\gamma\text{-Al}_2\text{O}_3$ .



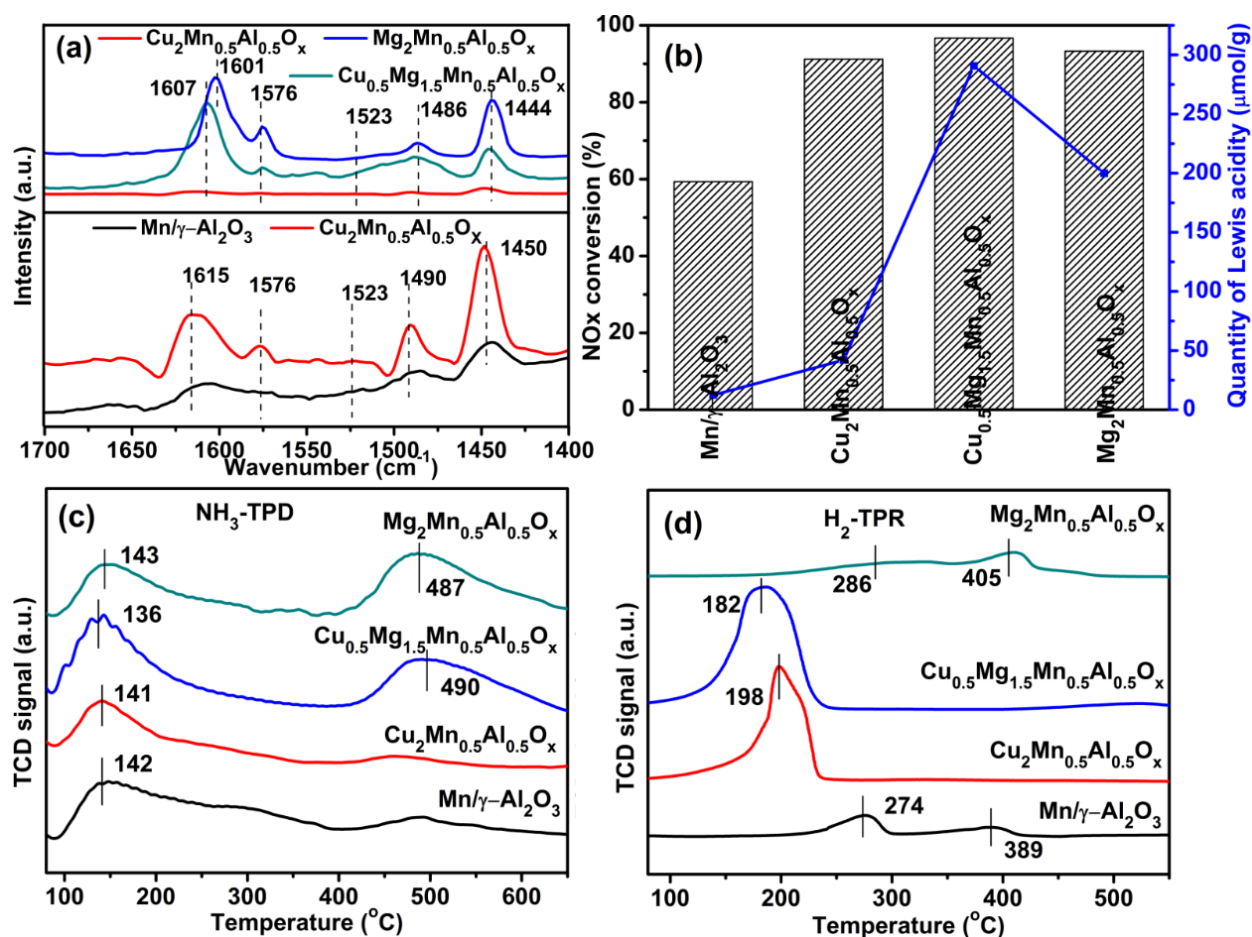


**Fig. 5.** (a) FTIR spectra of pyridine adsorbed at 150 °C on the catalysts, (b) Variations in the quantity of Lewis acidity and the catalytic performance of catalysts at 150 °C, (c) NH<sub>3</sub>-TPD profiles of catalysts, and (d) H<sub>2</sub>-TPR profiles over the  $\text{Cu}_2\text{Mn}_{0.5}\text{Al}_{0.5}\text{O}_x$ ,  $\text{Cu}_{0.5}\text{Mg}_{1.5}\text{Mn}_{0.5}\text{Al}_{0.5}\text{O}_x$ ,  $\text{Mg}_2\text{Mn}_{0.5}\text{Al}_{0.5}\text{O}_x$ , and  $\text{Mn}/\gamma\text{-Al}_2\text{O}_3$  catalysts.

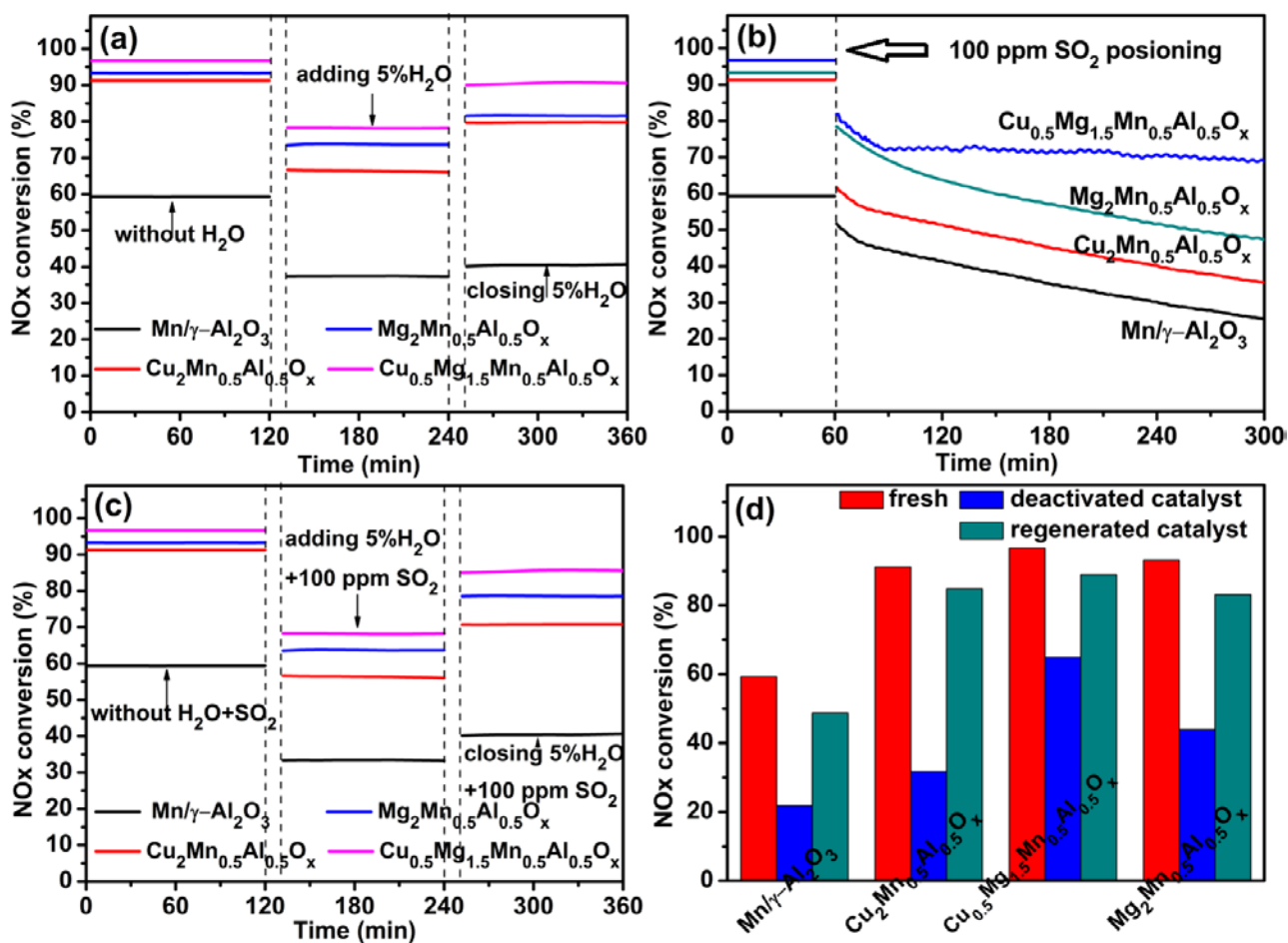


**Fig. 6.** (a) The effect of individual H<sub>2</sub>O, (b) The effect of individual SO<sub>2</sub>, and (c) the effect of SO<sub>2</sub> and H<sub>2</sub>O co-existence on the NO<sub>x</sub> conversions over catalysts at 150 °C, (d) NO<sub>x</sub> conversions of fresh, deactivated and regenerated catalysts treated by thermal regeneration. Reaction conditions: [NO<sub>x</sub>] = [NH<sub>3</sub>] = 500 ppm, [O<sub>2</sub>] = 5%, [H<sub>2</sub>O] = 5%, [SO<sub>2</sub>] = 100 ppm, balance Ar, total flow rate = 200 mL/min, GHSV=60,000 h<sup>-1</sup>, catalyst 0.15 g.

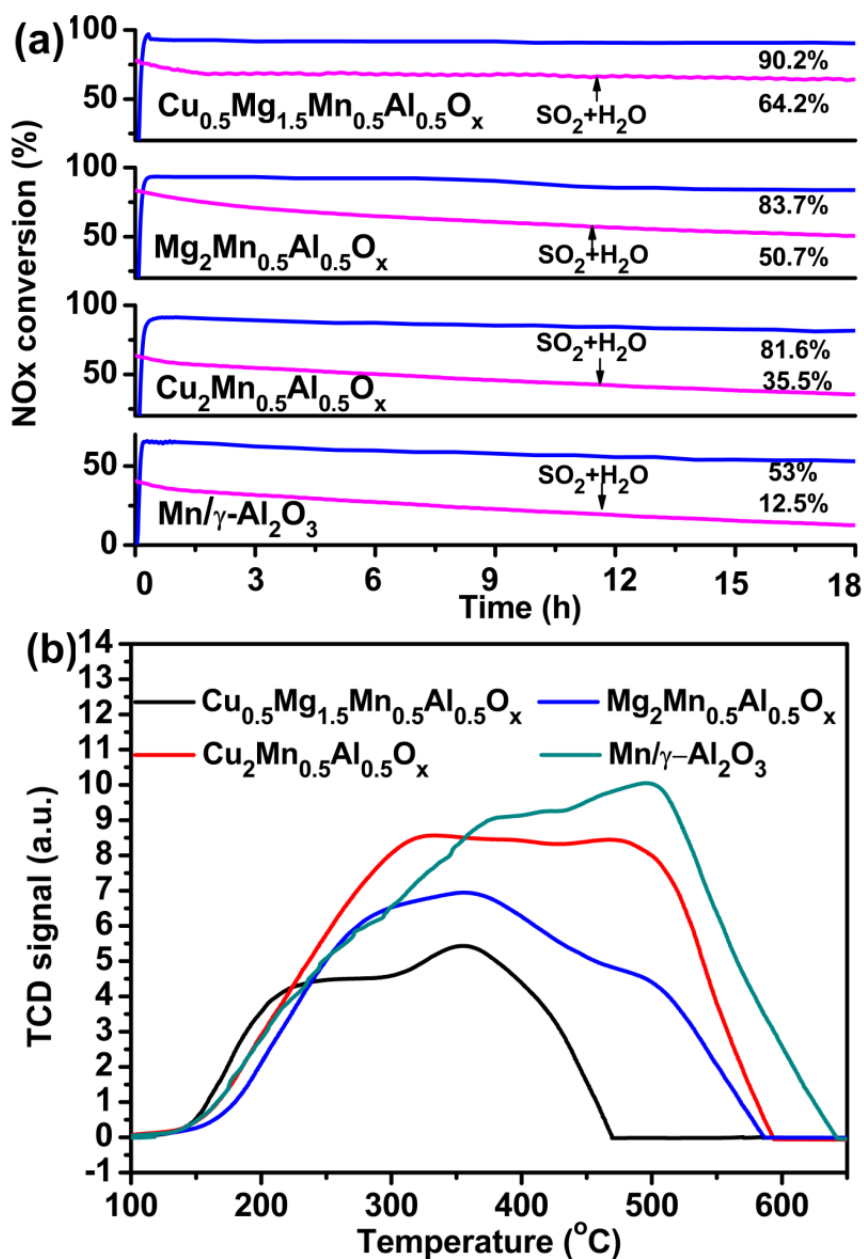


**Fig. 7.** (a) Long-time test with/without 100 ppm SO<sub>2</sub>+ 5% H<sub>2</sub>O of catalysts. Reaction conditions: [NO<sub>x</sub>] = [NH<sub>3</sub>] = 500 ppm, [O<sub>2</sub>] = 5%, [H<sub>2</sub>O] = 5% (if added), [SO<sub>2</sub>] = 100 ppm (if added), balance Ar, total flow rate = 200 mL/min, GHSV=60,000 h<sup>-1</sup>, catalyst 0.15 g, (b) SO<sub>2</sub>-TPD of pre-sulfated catalysts.

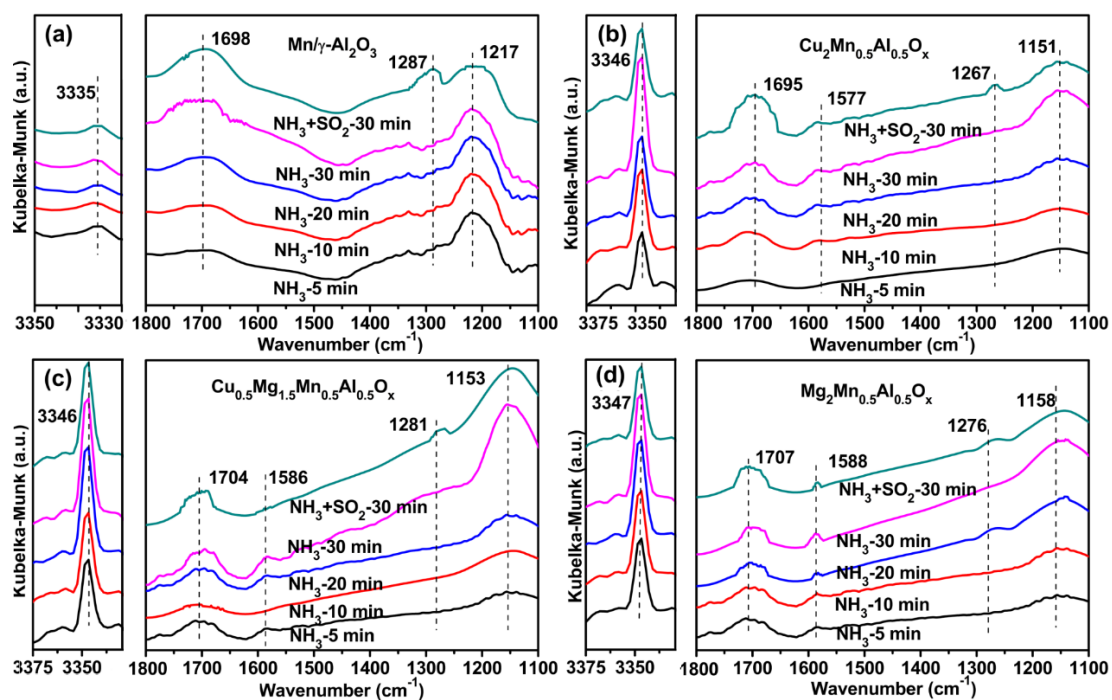


**Fig. 8.** In situ DRIFT spectra obtained after a 30 min exposure to NH<sub>3</sub> and NH<sub>3</sub> + SO<sub>2</sub> over a) Mn/ $\gamma$ -Al<sub>2</sub>O<sub>3</sub>, b) Cu<sub>2</sub>Mn<sub>0.5</sub>Al<sub>0.5</sub>O<sub>x</sub>, c) Cu<sub>0.5</sub>Mg<sub>1.5</sub>Mn<sub>0.5</sub>Al<sub>0.5</sub>O<sub>x</sub> and d) Mg<sub>2</sub>Mn<sub>0.5</sub>Al<sub>0.5</sub>O<sub>x</sub> catalysts at 150 °C.



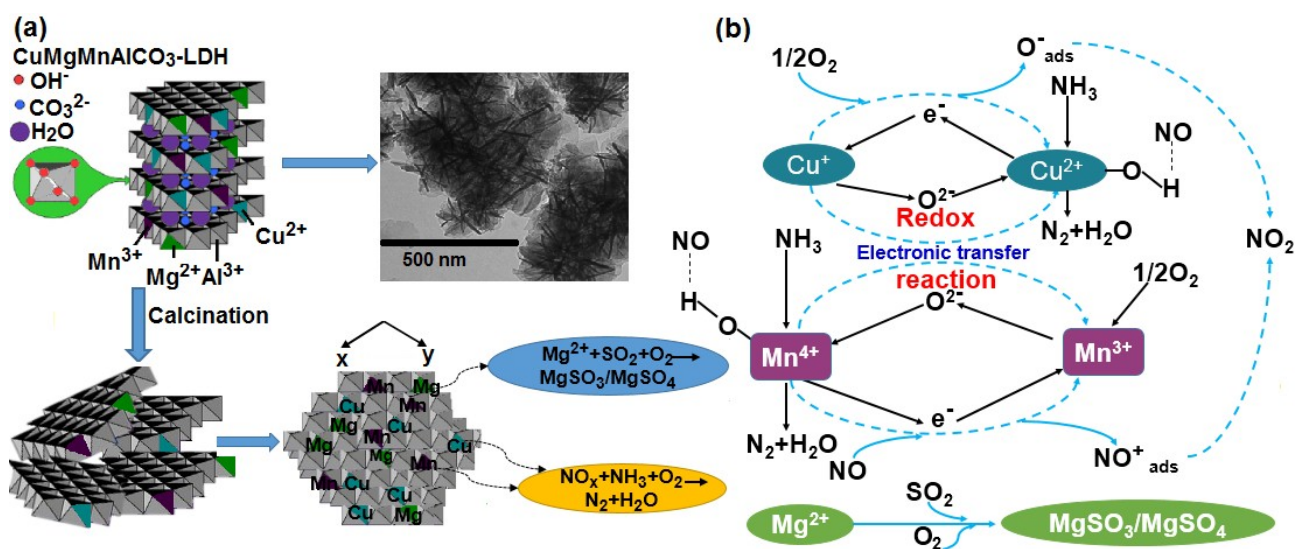


**Fig. 9.** (a) Schematic illustration of the preparation process of CuMgMnAlO<sub>x</sub>, and (b) A redox catalytic cycle of the low-temperature NH<sub>3</sub>-SCR reactions over CuMgMnAlO<sub>x</sub> catalysts.